

GANG CHEN is the Warren and Townley Rohsenow Professor at the Massachusetts Institute of Technology. He previously taught at Duke University and University of California at Los Angeles. His research and publications are in the areas of micro- and nanoscale heat transfer and energy conversion, with applications to microelectronics and microphotonics thermal management, thermoelectric thermal and solar photovoltaic energy conversion, and micro- and nanosystems. He is a recipient of the NSF Young Investigator Award, a Guggenheim Fellowship, and an ASME fellow. He serves on the editorial boards of several journals in heat transfer and nanotechnology, and as the chairman of the advisory board of the ASME Nanotechnology Institute.

in proofreading and figure drawing: D. Borca-Tasciuc, Z. Chen, J. Cybulski, C. Dames, T. Harris, A. Henry, L. Hu, A. Narayanaswamy, A. Schmidt, A. Shah, and, particularly, R.G. Yang, for summarizing students' comments. Several former students and post-docs are also acknowledged for stimulating me and contributing to my knowledge in the areas covered, including Drs T. Borca-Tasciuc, W.L. Liu, D. Song, S.G. Volz, B. Yang, and T.F. Zeng. Professors J.B. Freund (UIUC), P.M. Norris (U. Virginia), and M. Kaviany (U. Michigan) have provided constructive feedback on chapters of the book. I, of course, take responsibility for any mistakes. I would also acknowledge the K.C. Wong Education Foundation in Hong Kong and the Simon-Guggenheim Foundation for supporting my career at various stages. The inclusion of this book in the MIT-Papadopoulos Series in Mechanical Engineering would not have been possible without the generous support of Neil and Jane Papadopoulos and the series editors, Professors Rohan Abeyaratne and Nam Suh.

I would like to thank several funding agencies, including DOE, DARPA, JPL, NASA, NSF, and ONR, that provided support for my research in this area, among them particularly the NSF Young Investigator Award that supported my early career and the DOD/ONR Multidisciplinary University Research Initiative that provided me an opportunity to work across disciplines. This book is in many ways an integration of education and research. Several papers that I have written in the past few years were stimulated from making analogies between different energy carriers.

My editor at Oxford University Press, Danielle Christensen, put gentle pressure on me to finish the seemingly never-ending manuscript. Lisa Stallings and Barbara Brown at OUP were of great help in the production phase of the book. Sue Nicholls and Ian Guy at Keyword Publishing Services Ltd. carried out careful editing of the manuscript. My thanks go to them for turning the manuscript into final print.

I would like to thank my parents and my wife's parents for their moral support and prayers. Most of all my thanks go to my dear wife Tracy and our son and daughter, Andrew and Karen. I once read from the preface of a book in which the author (whom I know) claimed that on average every printed page of his book took three hours. I did not believe him until I came close to finishing this book. I started writing this book about five years ago, when we were expecting our daughter Karen and I changed my working habit to have a few hours in the early morning. I thought that the book could be finished as a gift at the birth of my daughter. That goal turned out to be a gross underestimation of the time needed to complete a book. Karen is now four and Andrew is ten. They have often been checking which chapter I was writing while waiting patiently with Tracy. A big portion of the roughly 1500 hours that I spent on the book was stolen from them. I hope the delivery of this manuscript will mean that I will now find more time to spend with them.

Figure C

Fig. 1.1(a) and (b): Copyrighted
Unauthorized use not permitted

Fig. 1.1(c): Reprinted with permission

Fig. 1.1(d): Reprinted with permission

Fig. 1.2(c): Reprinted with permission
"Thin-Film Thermoelectric Materials,"
Nature, vol. 413, pp. 597-598

Fig. 1.4(c): Reprinted with permission
pp. 1105-1107. Copyrighted

Fig. 2.6(a): Reprinted from
New York, with permission

Fig. 5.8: Reprinted with permission
Boundary Resistance," *Review of Physics and Chemistry*,
1989 by the American Physical Society

Fig. 5.15(b): Reprinted with permission
Lieber, C.M., 1998, "Atomic Scale Structure of
Carbon Nanotubes," *Nature*

Fig. 5.17(a): Reprinted with permission
"Experimental Investigation of the Effect of
Cryogenic Temperatures on the Mechanical Properties of
Aluminum," permission from ASME.

Fig. 5.17(b): Reprinted with permission
fer between Closely-Spaced Surfaces,"
permission from Elsevier

Fig. 8.6(a) and (b): Reprinted with permission
Mechanisms during Short-Duration Tests,"
vol. 115, pp. 835-841, with permission

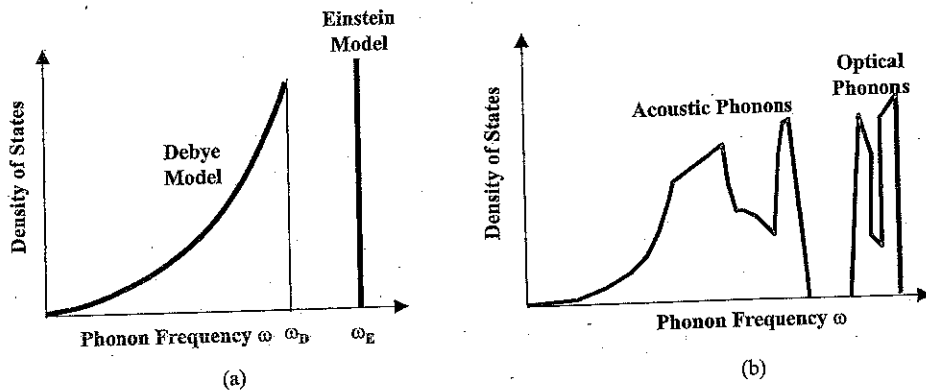


Figure 3.26 Phonon density of states, (a) approximated by the Debye and Einstein models and (b) in real crystals.

The densities of states for the Debye and Einstein models are illustrated in figure 3.26. The Debye model gives $D \propto \omega^2$, while the Einstein model gives a spike at ω_E . The densities of states in real crystals can be quite different from the predictions of these simple models, as illustrated in figure 3.26(b). At each frequency that the phonons intersect the zone boundary, a singularity, called the van Hove singularity, appears in the density of states because the dispersion curve is perpendicular to the zone boundary.

3.4.3 Photon Density of States

Photons also have a linear dispersion between frequency and wavevector, $\omega = ck$, which is identical to that of phonons under the Debye approximation. Consider an electromagnetic wave in a cubic box of length L . The electromagnetic fields can be decomposed into normal modes using Fourier series, as we did for phonons. The allowable wavevectors are then

$$k_x, k_y, k_z = 0, \pm 2\pi/L, \pm 4\pi/L, \dots \quad (3.58)$$

Hence, as before, photons share much commonality with phonons. However, significant differences exist: unlike phonon waves in a crystal, which have a minimum wavelength as imposed by the interatomic distance, no such a limit presents on the wavevector for photons. Following a derivation similar to phonons, we can obtain the density of states for an electromagnetic wave as

$$D(\omega) = \frac{dN}{Vd\omega} = \frac{\omega^2}{\pi^2 c^3} \quad (3.59)$$

One difference in the above equation from eq. (3.55) is that a factor of two rather than three is used to reflect the fact that electromagnetic waves (photons) have two transverse polarizations, whereas phonons can be longitudinally polarized as well. The other difference is that while the phonon density of states has a cut-off frequency given by the Debye frequency, photons do not have such a cutoff frequency.

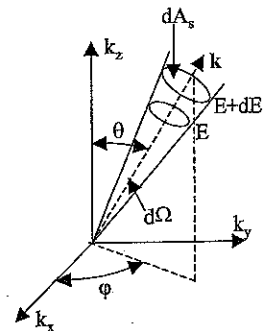


Figure 3.27

3.4.4 Differential Density of States

Although the density of states is a function of wavevector k or energy, we find it useful to define a differential density of states $dD(E, \mathbf{k})$ (figure 3.27)

where dA_s is a differential area element in k -space, and $d\Omega$ is a differential solid angle, defined in terms of the polar and azimuthal angles, θ and ϕ , of the specific wave vector direction \mathbf{k} .

$$dD(E, \mathbf{k}) = \frac{\text{No. of states}}{dE d\Omega dA_s}$$

where the second equality applies to photons.

3.5 Energy Levels

We touched upon quantum wells in the previous section. Structures can be made by various means, such as self-assembly. The energy states of these artificial structures often differ from those of bulk materials. The density of states of these structures is often different from that of bulk materials. One imposes new boundary conditions on the wavefunction, which other creates new periodicity, and thus new energy levels, in this section.

3.5.1 Quantum Wells

A quantum well can be formed by confining electrons in a thin layer. For example, a thin layer of

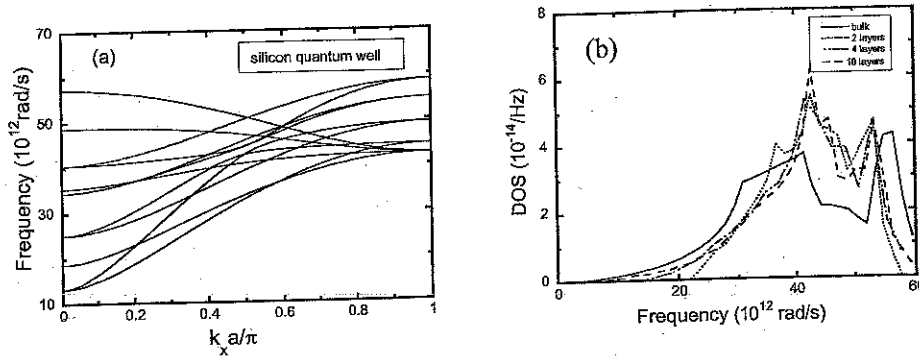


Figure 3.29 (a) Phonon dispersion and (b) density of states in quantum wells (Yang and Chen, 2000).

change can be seen experimentally through, for example, Raman spectroscopy, which probes the phonons through the frequency shift of a photon that interacts with a phonon (Weisbuch and Vinter, 1991). Numerous studies have been devoted to the effects of phonon confinement in quantum structures (Bannov et al., 1995). Recent applications include the use of phonon confinement to reduce thermal conductivity and thus, increase the thermoelectric energy conversion efficiency (Chen, 2001).

The quantum effects for nanometer-scale wires (quantum wires) and nanometer-scale dots (quantum dots) are expected to be even stronger than in quantum wells because of the additional boundary conditions on the electron or phonon motion in one or two more directions. A recent discovery is that of nanoscale tubular structures, particularly carbon nanotubes (Iijima, 1991). A carbon nanotube can be considered as the rolling of an atomic sheet (or several atomic sheets) of *graphitic* carbon (Dresselhaus et al., 2001). Graphite has a close-packed hexagonal structure, as shown in figure 3.5(c). The bonding between different layers is through the van der Waals bond, which is weaker than the covalent bonds within each layer. If only one atomic layer rolls up, the nanotube thus formed is called a single-walled carbon nanotube. If several layers roll up, the nanotube formed is called multiwalled. Depending on the nanotube diameter and the orientation of the major crystallographic directions with the nanotube axis, the nanotube can be a semiconductor or a metal, due to quantum size effects. The electron and phonon energy states in carbon nanotubes are very different from those in their bulk materials, leading to some special properties. The mechanical strength and thermal conductivity of these tubes are expected to be very high (Kim et al., 2001). Research is actively exploring various properties and applications of carbon nanotubes (Dresselhaus et al., 2001).

3.5.2 Artificial Periodic Structures

We have observed that the periodicity that naturally exists in bulk crystals plays a crucial rule in determining the electron and phonon energy levels. Natural systems are three dimensional, with a periodicity determined by the lattice constants. One can also create artificial periodic structures, for example, by repeatedly growing a thin layer of GaAs and a thin layer of AlAs on the same substrate. In fact, artificial periodic structures have been used widely in optical coatings, such as in the making of optical

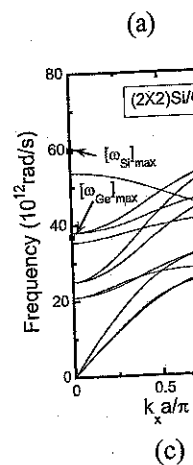
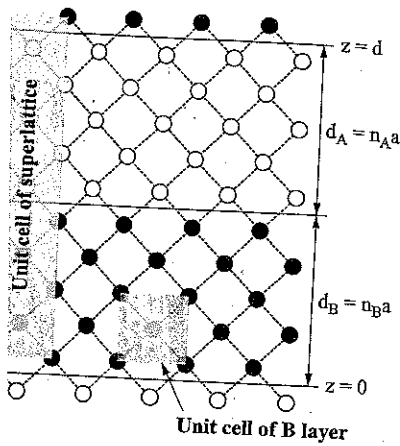


Figure 3.30 (a) A Si/Ge superlattice structure and (c) phonon dispersion (Chen, 2004).

interference filters that control light transmission (Heavens, 1965). An optical filter with a period thickness, as the order of the wavelength, We will discuss optical interference filters, periodic structures with the mean free path. Since the electron mean free path is short, such an analogy requires periodic structures. Consequently, the conventional thin film deposition technique is not suitable. Electron wave propagation in periodic structures can be analyzed using the Kronig-Penney model, leading to band structures very different from those of their constituent materials. These structures exhibit similar behavior, for example, in phonon spectra (Chen, 1979). Figure 3.30 shows the phonon spectra for acoustic phonons and the acoustic phonon dispersion



is still a and thus the maximum τ/a . In the cross-plane direction, the d represents the true periodicity in this direction that represents the lattice periodicity. The first Brillouin zone is π/d rather than π/a . The dispersion relations to those of the bulk material, a small gap, called a minigap, forms. This is due to the electronic gap formation in the superlattice because there are no bulk phonons; these phonons are confined inside the superlattice. One characteristic of the confined "acoustic" phonons is that the dispersion relation is similar to that of bulk silicon or germanium, but with a new unit cell that contains one silicon and one germanium atom. The new phonon or electron spectra, such as Kronig-Penney or harmonic oscillator, are longer than one period thickness.

In thin films have artificial periodicity, quantum wires and quantum dots, and superlattices that have artificial

artificial electronic bandgaps and phonon dispersion relations. These systems can sample and feel individual Brillouin zones, diffraction and interference effects. This is different from naturally existing crystals, since the Brillouin zone is averaged over a large volume of material. Quantum wells are made of alternating quarter-wavelength layers (alternating bands) along certain directions. The quantum well phenomenon corresponds to the

photon bandgap, similar to that in the Kronig-Penney model for electrons. By extending such a concept to three dimensions to make three-dimensional periodic structures with periods comparable to optical wavelength, Yablonovitch (1986) proposed the concept of three-dimensional photonic bandgap structures. These photonic crystals have become a very active research field and have potential applications in lasers, telecommunication, and optical coatings (Joannopoulos et al., 1995, 1997).

3.6 Summary of Chapter 3

The contents of this chapter are often covered, in a solid-state physics course, in at least three individual chapters: crystal structure, electronic energy states, and phonon energy states (Kittel, 1996; Ashcroft and Mermin, 1976). This condensed chapter introduces the terminology and often-used methodologies for the analysis of energy states in crystalline structures.

The most important characteristic of crystals is their periodicity, which is described by a lattice. Real crystals are obtained by attaching a basis to each lattice point. The basis can consist of one atom or a cluster of atoms. Lattices are described by the primitive lattice vectors. A primitive unit cell contains one lattice point, but a conventional unit cell can have more than one lattice point. One way to construct a primitive unit cell unambiguously is to form the Wigner-Seitz cell. In three-dimensional space, a total of 14 lattice types exists. The Miller index method is commonly used to denote crystal planes and directions.

A lattice is periodic in real space, and we often express a periodic function in terms of its Fourier transformation. The Fourier conjugate of real space is called the reciprocal space. The primitive lattice vectors in reciprocal space can be calculated from the primitive lattice vectors in real space. Diffraction experiments provide an image of reciprocal space. A Wigner-Seitz cell in reciprocal space is called the first Brillouin zone. Later, we express the energy dispersion of electrons and phonons in the ~~the~~ first Brillouin zone.

In a periodic structure, the electronic energy levels form energy bands. The band formation is demonstrated by the solution of the Schrödinger equation based on the Kronig-Penney model. In real crystals, each crystallographic direction has its own dispersion relation. The electronic band structure determines whether a material is metal, semiconductor, or insulator. In metals, an electronic band is only partially filled and electrons can move to the empty quantum states within the same band. The topmost electron energy level at 0 K is called the Fermi level. If a band is totally filled and the next band has an energy gap from this band, electrons cannot move within the band. Whether the electron can go to the next energy band depends on the magnitude of the bandgap compared to the thermal energy which is 26 meV at 300 K. A material can be a semiconductor if the bandgap is relatively small such that there exist some electrons with high enough energy to jump to the conduction band, leaving some vacant quantum states behind. If the bandgap is very large, no electrons can jump to the conduction band and the material is an insulator.

In a semiconductor, the motion of electrons in the valence band can be described by the motion of equivalent positive charges, called holes, that occupy the empty states in the band. Semiconductors can be intrinsic or extrinsic. Extrinsic semiconductors are obtained by adding impurities that have an energy level close to the conduction or

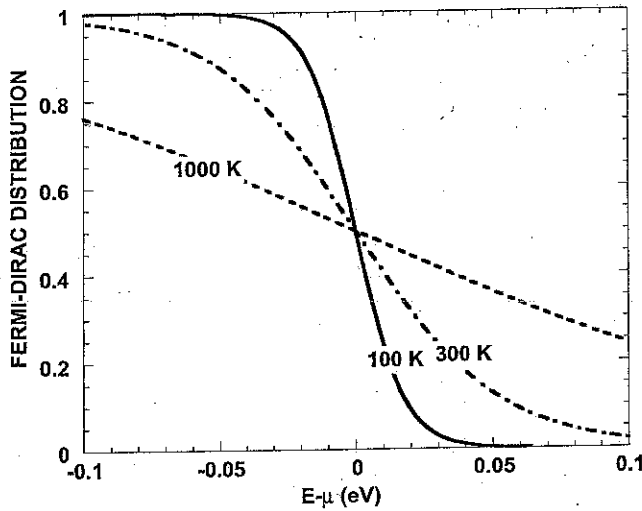


Figure 4.3 Fermi-Dirac distribution as a function of the electron energy relative to the chemical potential.

and, correspondingly, neither is the chemical potential. We know that for an accessible quantum state of the system, with frequency ν ; there can be an arbitrary number n of photons or phonons such that the total energy of this state is $E = (n + 1/2)h\nu$ ($n = 0, 1, 2, \dots$). Following a similar argument as for electrons, we take this quantum state to be our new system and the remaining quantum states to be the reservoir. Since neither the chemical potential nor the particle number is a thermodynamic variable, the new system is best described by a canonical ensemble with the canonical partition function

$$Z(\nu) = \sum_{n=0}^{\infty} \exp\left(-\frac{(n + 1/2)h\nu}{\kappa_B T}\right) = \frac{\exp\left(-\frac{h\nu}{2\kappa_B T}\right)}{1 - \exp\left(-\frac{h\nu}{\kappa_B T}\right)} \quad (4.40)$$

The probability that the quantum state (the new system) has n particles (photons or phonons) is thus

$$\hookrightarrow P(\nu, n) = \frac{\exp\left(-\frac{(n+1/2)h\nu}{\kappa_B T}\right)}{Z} = \exp\left(-\frac{nh\nu}{\kappa_B T}\right) \left[1 - \exp\left(-\frac{h\nu}{\kappa_B T}\right)\right] \quad (4.41)$$

and the average number of the particles, or the occupancy of the quantum state, is

$$\langle n \rangle \equiv f(\nu) = \sum_{n=0}^{\infty} n P(\nu, n) = \frac{1}{\exp\left(\frac{h\nu}{\kappa_B T}\right) - 1} \quad (4.42)$$

This equation is the *Bose-Einstein distribution function*, and the particles obeying this distribution are called *bosons*. Figure 4.4 shows the Bose-Einstein distribution. Because each particle has energy $h\nu$, the average energy of the quantum state is

$$\langle E \rangle = h\nu f(\nu) \quad (4.43)$$

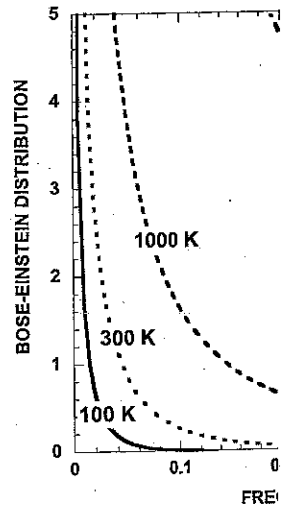


Figure 4.4 Bose-Einstein distribution as a function of the electron energy relative to the chemical potential.

where we have neglected the zero-point energy of the photons.

Other boson systems, such as gas molecules, also exhibit Bose-Einstein statistics. For such bosons, we should use the general Bose-Einstein distribution can be written as

$$\langle n \rangle \equiv f(E)$$

where μ is again the chemical potential.

The Bose-Einstein distribution changes over to the Fermi-Dirac distribution (at low temperature and high temperature), both Bose-Einstein and Fermi-Dirac distributions reduce to the Boltzmann distribution function

$$f(E, T, \mu) = \exp\left(-\frac{E - \mu}{\kappa_B T}\right)$$

This distribution function is considered the Boltzmann distribution. Bose-Einstein distributions are “quantum” and Fermi-Dirac distributions are “classical” and “quantum” statistics.

4.2 Internal Energy and Entropy

The statistical distribution functions for a quantum state and its energy level. We

Specific heat must be calculated from the format, eq. (4.56). Similarly, the specific heat is

$$\frac{c_v}{R} = \frac{5}{2} + \frac{\theta_r}{T} \left[\frac{\ell(\ell+1)}{3} - \frac{\theta_r \ell(\ell+1)}{3T} \right] \quad (4.58)$$

$$\frac{c_v}{R} = \frac{5}{2} + \frac{\theta_r}{T} \left[\frac{\ell(\ell+1)}{3} - \frac{\theta_r \ell(\ell+1)}{3T} \right] \quad (4.59)$$

theorem. After obtaining the complete total specific heat of a diatomic $C_V = C_{V,t} + C_{V,r} + C_{V,v} + C_{V,e}$.

characteristic temperature is 85.3 K and its vibrational degrees of freedom of hydrogen gas as a function of

we can write the total specific heat

$$\frac{c_v}{R} = \frac{5}{2} + \frac{\theta_r}{T} \left[\frac{\ell(\ell+1)}{3} - \frac{\theta_r \ell(\ell+1)}{3T} \right] \quad (E4.2.1)$$

is

$$\frac{c_v}{R} = \frac{5}{2} + \frac{\theta_r}{T} \left[\frac{\ell(\ell+1)}{3} - \frac{\theta_r \ell(\ell+1)}{3T} \right] \quad (E4.2.2)$$

summation. Figure E4.2 plots specific heat at various temperatures, only the translational degrees of freedom contribute at low temperatures (3R/2). As the temperature increases, vibrational degrees of freedom contribute to the specific heat and it reaches 5R/2. At even higher temperatures, electronic degrees of freedom start contributing to the specific heat.

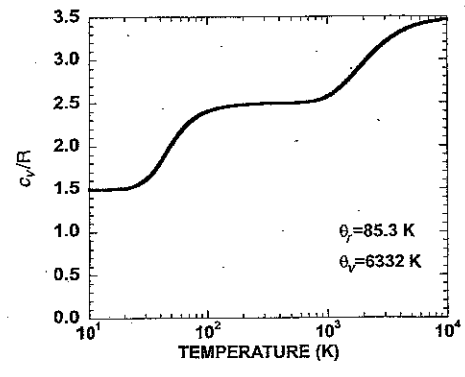


Figure E4.2 Specific heat of H₂ gas as a function of temperature.

4.2.2 Electrons in Crystals

Now we investigate the specific heat of electrons in a crystal. We assume that the electrons have a parabolic band with an isotropic effective mass

$$E - E_c = \frac{\hbar^2}{2m^*} (k_x^2 + k_y^2 + k_z^2) \quad (4.60)$$

We obtained the density of states in chapter 3, eq. (3.52),

$$D(E) = \frac{1}{2\pi^2} \left(\frac{2m^*}{\hbar^2} \right)^{3/2} (E - E_c)^{1/2} \quad (4.61)$$

The total number of electrons per unit volume is thus

$$n = \int_0^\infty f(E, T, \mu) D(E) dE \quad (4.62)$$

From eq. (4.62), the chemical potential as a function of temperature can be determined for a given n . For $T = 0$, the above relation leads to

$$n = \int_{E_c}^\mu D(E) dE = \frac{1}{3\pi^2} \left(\frac{2m^*}{\hbar^2} \right)^{3/2} (\mu - E_c)^{3/2} \quad (4.63)$$

We have already obtained this relation, eq. (3.53), in chapter 3. The chemical potential μ at $T = 0$ is called the Fermi level, E_f . At other temperatures, eq. (4.62) cannot be explicitly integrated. However, when $(E - \mu) / k_B T \gg 1$, which is the classical limit, we can use the Boltzmann distribution as an approximation of the Fermi-Dirac distribution. Equation (4.62) can be integrated explicitly,

$$n = \int_{E_c}^\infty \exp\left(\frac{-E + \mu}{\kappa_B T}\right) \frac{1}{2\pi^2} \left(\frac{2m^*}{\hbar^2} \right)^{3/2} (E - E_c)^{1/2} dE = N_c \exp\left(-\frac{E_c - \mu}{\kappa_B T}\right) \quad (4.64)$$

*In electronics, however, E_f is often used to represent the chemical potential at all temperatures.

with

$$N_c = 2 \left(\frac{2\pi m^* \kappa_B T}{h^2} \right)^{3/2} \quad (4.65)$$

Equation (4.64) is often used to determine the chemical potential level in doped semiconductors, as will be seen from the following example.

Example 4.3 Chemical potential level in doped semiconductors

Silicon is a widely used semiconductor material, and it is often doped with phosphorus to form an n-type semiconductor. Determine the chemical potential of an n-type semiconductor doped with phosphorus with a concentration of 10^{17} cm^{-3} at 300 K, assuming that every phosphorus atom contributes one free electron to the conduction band and neglecting thermally excited electrons from the valence band. Although the silicon conduction bands are not spherical [figure 3.18(b)], they can be approximated by an isotropic band with an effective mass equal to $0.33m$, where m is the free electron mass.

Solution: Silicon has six identical conduction bands [figure 3.18(b)]. When counting all six bands, eq. (4.64) should be written as

$$n = 12 \left(\frac{2\pi m^* \kappa_B T}{h^2} \right)^{3/2} \exp \left(-\frac{E_c - \mu}{\kappa_B T} \right) \quad (\text{E4.3.1})$$

Taking $n = 10^{17} \text{ cm}^{-3}$, we can find the chemical potential as

$$\begin{aligned} \frac{\mu - E_c}{\kappa_B T} &= \ln \left[\frac{n}{12} \left(\frac{2\pi m^* \kappa_B T}{h^2} \right)^{-3/2} \right] \\ &= \ln \left[\frac{10^{23}}{12} \left(\frac{2\pi \times 0.33 \times 9.1 \times 10^{-31} \times 1.38 \times 10^{-23} \times 300}{6.6^2 \times 10^{-68}} \right)^{-3/2} \right] \\ &= -5.65 \end{aligned} \quad (\text{E4.3.2})$$

Thus

$$\mu - E_c = -5.65 \times 26 \text{ meV} = -147 \text{ meV} \quad (\text{E4.3.3})$$

Comments. 1. The negative sign means that the chemical potential is below the conduction band edge. The silicon bandgap at room temperature is 1.12 eV. Thus the chemical potential level is within the bandgap. In fact, only in this case, the Boltzmann approximation we used in eq. (4.64) is applicable because the electron energy inside the conduction band, minus the chemical potential, is much larger than $\kappa_B T$. If the chemical potential is close to the band edge or falls

inside the conduction band, which is doped, we need to carry out numerical distribution.

2. The value of the chemical potential suggests that it is the relative difference in number density, and thus this distribution is discussed in chapter 6 (figure 6.9), we will point out this issue.

To calculate the specific heat of electrons as

$$U(T) =$$

For convenience, we limit our discussion to a unit volume n_e is fixed. We further

$$n_e = \int_0^\infty f(E) D(E) dE$$

We can use eq. (4.67) to rewrite eq.

$$U(T) = \int_0^\infty (E - E_f) D(E) f(E) dE$$

where E_f is the Fermi level (μ is dependent), we obtain the heat capacity

$$C_e = \int_0^\infty (E - E_f) D(E) f(E) dE$$

Typically, df/dT is nonzero only near E_f . If the density of states does not vary rapidly with energy, $D(\mu)$ can be taken out of the integration. In a very small band, E_f is very close to μ and set $\mu \approx E_f$. Under these

$$C_e \approx D(\mu) \int_0^\infty (E - E_f) f(E) dE$$

$$= D(\mu) \int_0^\infty (E - E_f) f(E) dE$$

$$\approx \kappa_B^2 T D(E_f)$$

- 4.3 *Specific heat of monatomic gas.* Derive an expression for the specific heat of a box of He gas and plot it as a function of temperature.
- 4.4 *Entropy of mixing.* There are two tanks of gas. Both tanks have N molecules and a volume V , and are at the same temperature and pressure. The two tanks are connected by a pipe with a valve. After the valve is opened, the gases in both tanks eventually mix into a homogeneous mixture. Show the following:
- If the two gases are identical, there is no change in entropy due to the mixing.
 - If the two gases are different, the mixing causes an entropy production of $2N \ln 2$.
- The difference in the results is called the Gibbs paradox and comes from the distinguishability of the molecules.
- 4.5 *Bose-Einstein distribution.* Plot the Bose-Einstein distribution as a function of frequency for $T = 100$ K, 300 K, and 1000 K. Compare with the Boltzmann distribution at the same temperatures.
- 4.6 *Electrons in semiconductors.* A semiconductor has a parabolic band structure

$$E - E_c = \frac{\hbar^2}{2m^*} (k_x^2 + k_y^2 + k_z^2)$$

The Fermi level in the semiconductor could be above or below the conduction band edge. Take the electron effective mass as the free electron mass. For $\mu - E_c = 0.05$ eV and $T = 300$ K, do the following in the range 0.0 eV $< E - E_c < 0.1$ eV:

- Plot the Fermi-Dirac distribution as a function of E ,
 - Plot the density of states as a function of E ,
 - Calculate the product of $f(E, T)D(E)$, which means the average number of electrons at each E , and plot the product as a function of E ,
 - Calculate the product of $E f(E, T)D(E)$, which means the actual energy at each allowable energy level, and plot the product as a function of E .
- Repeat the questions for $\mu - E_c = -0.05$ eV.

- 4.7 *Chemical potential.* The number of electrons in the conduction band can be assumed to be equal to the dopant concentration. Calculate the chemical potential levels relative to the band edge for the dopant concentrations of 10^{18} cm $^{-3}$ and 10^{19} cm $^{-3}$, assuming free electron mass and $T = 300$ K.
- 4.8 *Debye crystal.* A crystal has a Debye velocity of 5000 ms $^{-1}$, and a Debye temperature of 500 K. For $T = 300$ K,
- Plot the Bose-Einstein distribution as a function of ω ,
 - Plot the density of states as a function ω using the Debye model.
 - Plot fD as a function of frequency ω .
 - Plot $\hbar\omega fD$ as a function of ω .
 - Compute the specific heat of the crystal as a function of temperature for $1 < T < 1000$ K.
- 4.9 *Blackbody radiation.* Consider the blackbody radiation at $T = 300$ K.
- Plot the Bose-Einstein distribution as a function of angular frequency ω .
 - Plot the density of states as a function of ω , using the Debye model.
 - Plot fD as a function of ω .
 - Plot $\hbar\omega fD$ as a function of ω .

- Compute the emi corresponding specific heat
 - Also compare (a) problem 4.8.
- 4.10 *Specific heat of diatomic energy state at 100 meV contribution of this molecule as a function of temperature*
- 4.11 *Electron specific heat of energy and specific heat \AA and 100\AA , as a function to the free electron mass*
- 4.12 *Electron specific heat of energy and specific heat height with $L = 20 \text{\AA}$ or effective mass equal to $2 \times 10^{28} \text{ m}^{-3}$.*
- 4.13 *Phonon specific heat. f relation (three-dimensio*

where a is the lattice c
Derive an expression for

- 4.14 *Fermi level and specific is $5.9 \times 10^{22} \text{ cm}^{-3}$.*
- Calculate the Fermi
 - What is the corres
 - Estimate the elect
 - Calculate the Ferr
- 4.15 *Phonon specific heat in per basis and a lattice theorem, estimate the p temperatures and comp.*
- 4.16 *Phonon high temperat temperatures the Deby the number of atoms in*
- 4.17 *Diamond specific heat. the specific heat of dia (the lattice constant of*
- 4.18 *Phonon specific heat in 5000 ms^{-1} and a Deb quantum dot obey the s considering the discret a cubic quantum dot wi the specific heat of the*

- 4.19 *Blackbody radiation in a small cavity.* Consider thermal radiation in equilibrium inside ~~such~~ a cubic cavity. Compute the radiation energy density in a cubic cavity of length $L = 1 \mu\text{m}$ at $T = 400 \text{ K}$ and compare it with the Planck distribution obtained by assuming that the cavity is very large compared to the wavelength.
- 4.20 *Entropy of one phonon state.* From eqs. (4.14) and (4.40), show that the entropy, s , of one phonon state having a frequency ω obeys the following relationship:

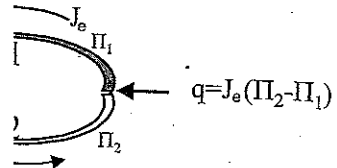
$$\frac{\hbar\omega}{T} f_0(1 + f_0) = -\frac{\kappa_B T}{\hbar} \frac{\partial s}{\partial \omega}$$

Where f_0 is the Bose-Einstein distribution.

The wave-particle duality of matter has been discussed in previous chapters. Particles such as electrons and photons have both wave and particle characteristics. In this chapter, we discuss material waves are granular rather than continuous. A frequency ν contains a discrete number of quanta. A fundamental property of waves is a fixed relationship between two quantities: phase and frequency. This phase relationship, the superposition principle, and diffraction phenomena that

The wave characteristics of matter are important for transport processes at interfaces. In previous chapters that the size effects of matter are the formation of standing waves at a single interface, and multilayers. We will make use of the wave characteristics of electrons, photons, and phonons. In chapter 3 the electron waves based on the wave-particle duality are readily observable and can be described by the Maxwell equations, which will be used in a continuum approach based on the dynamics method we used in chapter 2. We will treat phonons in parallel with electrons, interference, and tunneling phenomena. The descriptions of these phenomena will be based on their statistical behavior, dispersion

3/29/66



$$\begin{aligned}
 &= -J_e \frac{d\Pi}{dT} \frac{dT}{dx} + \frac{d}{dx} \left(k \frac{dT}{dx} \right) - S J_e \left(\frac{dT}{dx} \right) + J_e \frac{d\Phi}{dx} \left(\frac{J_e}{\sigma} \right) \\
 &= - \left(T \frac{dS}{dT} \right) J_e \frac{dT}{dx} + \frac{d}{dx} \left(k \frac{dT}{dx} \right) + \frac{J_e^2}{\sigma}
 \end{aligned}
 \tag{6.105}$$

In the above derivation we have used eqs. (6.91), (6.103), and (6.104). In the last equation, the second term is due to heat conduction and the third term is due to Joule heating. These two terms are quite familiar in a heat conduction equation. The first term, however, is not familiar. It shows that heat can be absorbed or released, depending on the current direction. This reversible heat absorption or rejection is called the Thomson effect. The *Thomson coefficient* [$V K^{-1}$] is defined as the rate of cooling

$$\beta = \dot{q}_c / \left(J_e \frac{dT}{dx} \right) = T \frac{dS}{dT}
 \tag{6.106}$$

where the negative sign in the first term of eq. (6.105) does not appear because a positive Thomson effect is based on cooling whereas \dot{q} is the heat generation. Equations (6.104) and (6.106), relating the three thermoelectric coefficients, S , Π , and β , are called the Kelvin relations.

Throughout this section, we have seen that the transport coefficients are often related, as for example in the Kelvin relations between the thermoelectric coefficients and the Einstein relation for the electrical diffusivity and the mobility. The fact that many of these coefficients are related has a more profound origin than a result from the Boltzmann equation. It is a requirement of the "time reversal invariance" of the mechanical equations of motion, that is, the particles retrace their former paths if all velocities are reversed. On the basis of this principle, Onsager (1931) derived the famous *Onsager reciprocity relations*. Here we will give a brief explanation of the reciprocity relations without proof (Callen, 1985). The flux of any extensive variable of a system (such as energy flux, particle flux) or at a local point of a system can be expressed as a linear combination of all the generalized driving forces F_j .

$$J_k = \sum_j L_{jk} F_j
 \tag{6.107}$$

where L_{jk} are called the kinetic coefficients. The generalized forces are the driving forces for entropy production. The Onsager reciprocal relations are

$$L_{jk} = L_{kj}
 \tag{6.108}$$

For local thermoelectric transport, the generalized forces are $\nabla(1/T)$ for heat flow and $(-\nabla\Phi)/T$ for electrical current, which leads to a relation between the two coefficients L_{12} and L_{21} as given by eq. (6.101).

Example 6.1

The relaxation time usually depends on the electron energy as $\tau \sim E^\gamma$, where γ differs among scattering mechanisms for electron transport ($\gamma = -1/2$ for acoustic phonon scattering, $\gamma = 1/2$ for optical phonon scattering, and $\gamma = 3/2$ for impurity scattering). Derive an expression for the Seebeck coefficient of a nondegenerate semiconductor.

$$D(E)dE
 \tag{6.102}$$

and (6.100) leads to

$$\Pi J_e - k \frac{dT}{dx}
 \tag{6.103}$$

$$\frac{L_{21}}{L_{11}}
 \tag{6.104}$$

ronic thermal conductivity. Seebeck coefficient is one of the

heat conduction by electrons, related to the current. When two regions of the junction, heat must be transferred between the Peltier effect and the energy absorbed ($q > 0$)

heat depends on the current. The Peltier effect is reversible. This effect is used in thermoelectric pumps (Goldsmid, 1986). It leads to reversible heating or cooling. If a temperature gradient and an electrical volume along the conduction axis and the electrochemical

$$\frac{d\Phi}{dx}$$

Solution: A nondegenerate semiconductor is one with the Fermi level inside the bandgap. In this case, the Fermi–Dirac distribution function can be approximated by the Boltzmann distribution

$$f = \frac{1}{\exp\left(\frac{E-E_f}{\kappa_B T}\right) + 1} \approx \exp\left(-\frac{E-E_f}{\kappa_B T}\right) \quad (E6.1.1)$$

The Seebeck coefficient can be calculated from eq. (6.94). Assuming a parabolic band, the density of states is

$$D(E) = \frac{1}{2\pi^2} \left(\frac{2m^*}{\hbar^2}\right)^{3/2} E^{1/2} \quad (E6.1.2)$$

Substituting (E6.1.2) and the relaxation time into eq. (6.94), we obtain the Seebeck coefficient as

$$S = -\frac{1}{eT} \frac{\int_0^\infty (E-E_f) E^{\gamma+3/2} \exp\left(-\frac{E-E_f}{\kappa_B T}\right) dE}{\int_0^\infty E^{\gamma+3/2} \exp\left(-\frac{E-E_f}{\kappa_B T}\right) dE} = -\frac{\kappa_B}{e} \left[-\frac{E_f}{\kappa_B T} \mathcal{F}\left(\gamma + \frac{5}{2}\right) \right] \quad (E6.1.3)$$

where E_f is the chemical potential, which can be controlled by doping. Using eq. (4.64) ($E_c = 0$ for the reference system here), we can write the above equation as

$$S = -\frac{\kappa_B}{e} \left[\ln\left(\frac{n}{N_c}\right) \mathcal{F}\left(\gamma + \frac{5}{2}\right) \right] \quad (E6.1.4)$$

Comment. The value of κ_B/e is $86 \mu\text{V K}^{-1}$, which gives an idea of the order of the magnitude of the Seebeck coefficient in many materials.

6.3.5 Hyperbolic Heat Conduction Equation and Its Validity

One assumption we made in the derivation of the classical constitutive equations, such as the Fourier law, is that the transient effect on the distribution function is negligible,

$$\tau \frac{\partial f}{\partial t} \ll \tau \mathbf{v} \cdot \nabla f \quad (6.109)$$

This will be valid if the variation of the distribution function in the time scale is much smaller than the variation of the distribution function in the length scale. Now, let's relax this approximation but still make the assumption that deviation from spatial equilibrium is small. Equation (6.49) becomes

$$\tau \frac{\partial f}{\partial t} + f = f_0 - \tau \left(\mathbf{v} \cdot \nabla_{\mathbf{r}} f_0 + \frac{\mathbf{F}}{m} \cdot \nabla_{\mathbf{v}} f_0 \right) \quad (6.110)$$

Let's consider one-dim the force term. We can tra of the left- and right-hand

$$\int_{4\pi} \left[\int_{4\pi} \dots \right] = \int_{4\pi} \dots$$

where we have used 4π over all directions. Eq. (6.1

where $\bar{\tau}$ is a weighted aver. Equation (6.112) is the Ca Tamma and Zhou, 1997). C (no heat generation consid

and eliminating J_q , we ar distribution

This is a *hyperbolic* type of heat conduction equation c term on the left-hand side temperature perturbation is the whole region (the tem not absolutely zero). The h since the heat propagation the other side of the wave existence of the second ter there are also other accepte and Preziosi, 1989),

where k_1 is another physic We comment here that a speed of Fourier's heat cor cable. There are many mat

6.9 Exercises

6.1 *Phonon thermal conductivity at intermediate temperature.* The phonon-phonon scattering relaxation time in the intermediate range of temperature (when $T < \theta_D$) can be approximated as

$$\frac{1}{\tau} = A \exp\left[-\frac{\Theta}{aT}\right] T^3 \omega^2$$

On the basis of the Debye model (linear dispersion), derive an expression for the thermal conductivity and discuss its dependence on temperature.

6.2 *High-temperature thermal conductivity.* At high temperature, the phonon relaxation time in a crystal is

$$\frac{1}{\tau} = \frac{\kappa_B T}{mva}$$

where a is of the order of distance between atoms and m is the atomic weight.

(a) Prove that the high-temperature thermal conductivity is proportional to $1/T$.

(b) The thermal conductivity of silicon at 300 K is $145 \text{ W m}^{-1} \text{ K}^{-1}$. Estimate its thermal conductivity at 400 K.

6.3 *Rosseland diffusion approximation for photon transport.* Consider an absorbing and emitting medium for thermal radiation transport. When the photon mean free path is much smaller than the characteristic length in the transport direction, the local equilibrium approximation is valid. Prove that under this condition (called optically thick) the radiative heat flux can be expressed as

$$q = -\frac{4\pi}{3\alpha} \frac{dI_b}{dx}$$

where α is the absorption coefficient. This is called the Rosseland diffusion approximation.

6.4 *Wiedemann-Franz law.* The electrical resistivity of gold at 300 K is $3.107 \times 10^{-8} \Omega \text{ m}$. Estimate its thermal conductivity.

6.5 *Wiedemann-Franz law.* The thermal conductivity of copper is $401 \text{ W m}^{-1} \text{ K}^{-1}$ at 300 K. Estimate its electrical conductivity at the same temperature.

6.6 *Energy and momentum relaxation time.* The electrical resistivity and thermal conductivity of gold at 300 K are $3.107 \times 10^{-8} \Omega \text{ m}$ and $315 \text{ W m}^{-1} \text{ K}^{-1}$. Estimate the momentum and energy relaxation time, and the momentum and energy relaxation length, of electrons in gold.

6.7 *Thermal conductivity and viscosity.* The thermal conductivity of air is $0.025 \text{ W m}^{-1} \text{ K}^{-1}$. Estimate its dynamic viscosity.

6.8 *Electrons in semiconductors.* An n-type semiconductor has a carrier concentration of 10^{18} cm^{-3} and a mobility of $200 \text{ cm}^2 \text{ V}^{-1} \text{ s}^{-1}$ at 300 K. Estimate the following: (a) electrical conductivity; (b) electron diffusivity; (c) momentum relaxation time; and (d) electron mean free path. Take the electron effective mass as that of a free electron.

Quantum Well Structures," *Journal of Heat Generation and Transport in Transfer*, vol. 117, pp. 25-31. London, North-Holland, Amsterdam. Conductivity, Second Sound, and Crystals," *Physical Review*, vol. 148, chapters 7 and 11, IEEE Press, Physical Review, vol. 132, on Thermal Conductivity Studies," *Review of Modern Physics*, vol. 61, on Films with Thickness of Order 7. ional Modes," *Solid State Physics, sics II, Nonequilibrium Statistical nd Electrical Modeling of Sub-*, vol. 79, pp. 7353-7361. "I," *Journal of Physics (Moscow)*, chapter 6, Pergamon, Oxford. -341, Wiley, New York. ed., chapters 2 and 7, Cambridge ric Thin Films," *Journal of Heat ond Sound in Bismuth*," *Physical es I*," *Physical Review*, vol. 37, ung in Kristallen," *Annalen der ing Short-Pulse Laser Heating of hysics*, p. 527, McGraw-Hill, *Heat Transfer*, Hemisphere, York. Thermal Transport and Thermo-," *Journal of Thermal Stress, il Gas Dynamics*, pp. 325-348, Mechanical Effect at Very Low Press, Oxford.

- 6.9 *Thermal conductivity of gases.* Prove that the thermal conductivity of a dilute monatomic gas is

$$k = \frac{5}{2} \left(\frac{\kappa_B}{m} \right) n \tau \kappa_B T$$

- 6.10 *Thermoelectric cooler.* A thermoelectric device is typically made of p-n junctions as shown in figure P6.10. When a current flows through the p-n junction, both electrons and holes carry energy from the cold side to the hot side. The Peltier coefficients of both p and n materials are equal in magnitude, Π , but of opposite sign. The cooling rate due to current flow is $2\Pi \times I$. In addition to this cooling, there is also Joule heating and reverse heat conduction. Assuming that the electrical and thermal conductivities of both legs are the same, derive an expression for the net cooling power at the cold side in terms of the temperatures at the cold and the hot side, the current, and the cross-sectional area and length of the leg. Show that the cooling power reaches a maximum at a certain optimum current value.

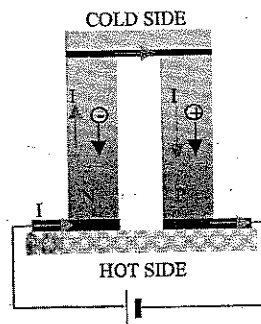


Figure P6.10 Figure for problem 6.10.

- 6.11 *Seebeck coefficients of a quantum well.* Derive an expression for the Seebeck coefficient of a quantum well of well-width d and with an infinite potential barrier height, as a function of the doping concentration.
- 6.12 *Power factor of a quantum well.* Because of Joule heating and reverse heat conduction, the efficiency of a thermoelectric device is determined by the figure of merit, defined as $Z = S^2\sigma/k$, where S is the Seebeck coefficient, σ the electrical conductivity, and k the thermal conductivity. The numerator $S^2\sigma$ is also called the power factor.

(a) Derive an expression for the power factor $S^2\sigma$ for a quantum well of width d and with an infinite barrier height, in terms of electron effective mass, relaxation time, chemical potential, and quantum well width.

(b) Assuming constant relaxation time and Boltzmann distribution, simplify the results obtained.

- 6.13 *Seebeck coefficient of nondegenerate silicon.* For silicon with doping concentration between 10^{16} and 10^{18} cm^{-3} , the Boltzmann distribution can be used instead of the Fermi-Dirac distribution. Silicon has six identical conduction bands with an effective mass of $0.33 m_e$ for each conduction band, where m_e is the mass of a free electron. Assume a constant relaxation time. \downarrow At $T=300\text{K}$

- (a) Calculate the Fermi energy E_F . How does the Fermi-Dirac and the Boltzmann distribution differ much in the given case?
- (b) Calculate the Seebeck coefficient S .
- 6.14 *Seebeck coefficient of a metal.*
- (a) Assuming a constant relaxation time τ of a metal is given by

(b) Prove that ZT for a

- (c) Estimate the Seebeck coefficient S .
- 6.15 *Einstein relation.* When the Einstein relation between mobility μ and

conductivity of a dilute

(a) Calculate the Fermi level as a function of the carrier concentration from both the Fermi-Dirac and the Boltzmann distribution, and show that the levels do not differ much in the given doping range.

(b) Calculate the Seebeck coefficient as a function of the dopant concentration.

6.14 Seebeck coefficient of a metal.

(a) Assuming a constant relaxation time, prove that the Seebeck coefficient of a metal is given by

$$|S| = \frac{\pi^2 k_B^2 T}{2eE_f}$$

(b) Prove that ZT for a metal satisfies the following inequality

$$ZT \leq \frac{3\pi^2 k_B^2 T^2}{4E_f^2}$$

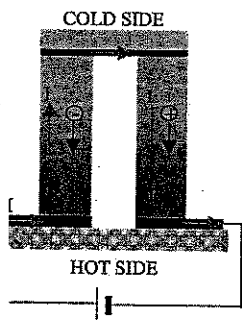
at 300 K

(c) Estimate the Seebeck coefficient of copper

6.15 Einstein relation. When the Boltzmann approximation is valid, prove the Einstein relation between mobility and diffusivity for electrons

$$a = \frac{k_B T}{e} \mu$$

ally made of p-n junction through the p-n junction, le to the hot side. The magnitude, Π , but of $\Pi \times I$. In addition to conduction. Assuming are the same, derive an ms of the temperatures ctional area and length m at a certain optimum



ssion for the Seebeck h an infinite potential

ating and reverse heat terminated by the figure eck coefficient, σ the The numerator $S^2 \sigma$ is

quantum well of width ective mass, relaxation

tribution, simplify the

with doping concen- tribution can be used identical conduction uction band, where ation time.

At $T=300K$

le Reynolds Lubrication Equation with 3, pp. 2237–2244.
 essive Improvement of the Modified sfer,” *Journal of Thermophysics and*

Diffusive Equations for Multidimen- the 2002 *International Heat Transfer* le, France.

Simulation of Nanoscale Multidi- Ballistic-Diffusive Equations and ss.

in Thin Films: Impacts of Thermal *Journal of Heat Transfer*, vol. 123,

s, Oxford, chapter 11.

conductivity of thin films with a freestanding thin film, starting boundary is specularly reflecting bulk thermal conductivity of the

luctivity of thin films with diffuse s ~2500 Å. Estimate the thermal ilicon membrane at room tem- diffusely. The room temperature -1.

iffuse surfaces on the electrical t for the electrical conductivity ter electrons partially diffusely fraction of specularly scattered

ffuse surfaces on the electronic n films. Derive an expression onductivity along a thin film, artially diffusely and partially specularly scattered electrons.

ck coefficient along a thin film. t along a thin film, assuming e Seebeck coefficient higher or at of the bulk material for the

urfaces on the Seebeck coeffi- ie Seebeck coefficient along a

thin film, assuming that the interfaces scatter electrons partially diffusely and partially specularly, with p representing the fraction of specularly scattered electrons. Neglect quantum size effects.

7.7 *Size effect on the phonon thermal conductivity along a circular nanowire.* Derive an expression for the effective phonon thermal conductivity of a circular nanowire, *assuming diffuse interface scattering.*

7.8 *Size effect on the phonon thermal conductivity of a square nanowire.* Derive an expression for the effective phonon thermal conductivity of a square nanowire, *assig*

7.9 *Phonon transport perpendicular to interfaces of thin films.* A thin film is sandwiched between two identical cladding materials. The parent material of the film has a thermal conductivity of $k_1 = 145 \text{ W m}^{-1} \text{ K}^{-1}$, $v_1 = 6400 \text{ m s}^{-1}$, and $C_1 = 1.66 \times 10^6 \text{ J m}^{-3} \text{ K}^{-1}$. The cladding materials have the following properties: $v = 3900 \text{ m s}^{-1}$, $C = 1.67 \times 10^6 \text{ J m}^{-3} \text{ K}^{-1}$. Estimate the effective thermal conductivity in the direction perpendicular to the film as a function of the film thickness for the film thickness in the range of 10–1000 Å, taking the phonon reflection at the two interfaces into consideration. *diffuse interface scattering.*

7.10 *Rarefied gas heat conduction.* Extend the diffusion approximation, together with appropriate boundary conditions for partially accommodating surfaces, for heat conduction through a gas sandwiched between two parallel plates. Derive an expression for the effective thermal conductivity of the gas as a function of the accommodation coefficients on the two surfaces and the Knudsen number.

7.11 *Rarefied Couette flow.* Derive an expression for the velocity distribution using the slip boundary condition, eq. (7.145) for Couette flow, as shown in figure P7.11. The bottom plate is stationary and the top plate is moving at constant speed U_0 .

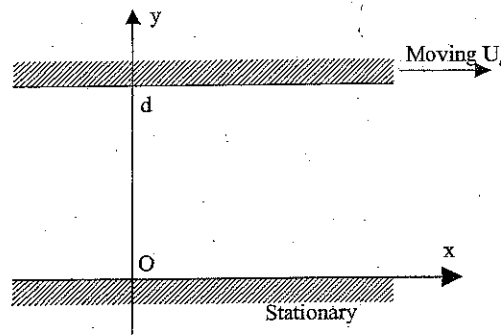
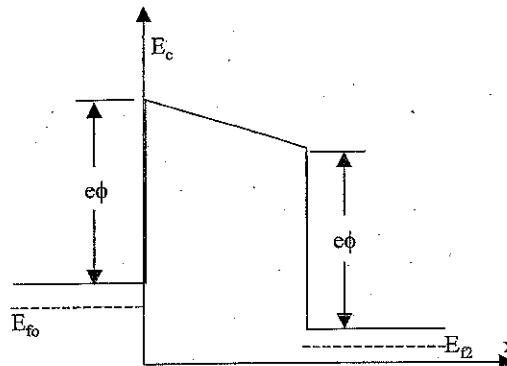


Figure P7.11 Figure for problem 7.11, Couette flow.

7.12 *Electrical conductivity of a double heterojunction structure.* A semiconductor thin film sandwiched between two semiconductor materials has two interfaces and is called a double heterojunction (see figure p7.12). Extend the drift-diffusion approximation, with the diffusion–transmission boundary condition, for electrical conductivity perpendicular to a thin film with a barrier height ϕ at both interfaces. Neglect quantum size effects on the electron energy levels, and the electrostatic potential change due to the depletion or accumulation of electrons in the barrier region.

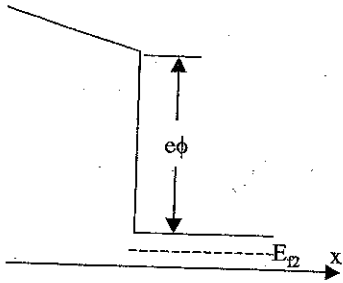
Figure P7.12 Figure for problem 7.12, thermionic emission.



- 7.13 Radiative heat transfer between two concentric spheres. Apply the modified differential approximation to solve the problem of radiative heat transfer between two concentric spheres maintained at two different temperatures T_1 and T_2 . Assume each wall is black and the gas between the shells is absorbing, emitting, and isotropically scattering.
- 7.14 Radiative heat transfer between two concentric cylinders. Apply the modified differential approximation to solve the problem of radiative heat transfer between two concentric cylinders maintained at two different temperatures T_1 and T_2 . Assume each wall is black and the gas between the cylinders is absorbing, emitting, and isotropically scattering.
- 7.15 Size effects of heat conduction across a cylindrical thin shell. Apply the ballistic-diffusive equations to solve the problem of steady-state phonon heat conduction between a cylindrical thin shell of thickness d . Derive an expression for the temperature distribution in the thin shell. The equivalent equilibrium temperatures at the inner and the outer surfaces are T_i and T_o , respectively. Phonon mean free path in the parent bulk material of the shell is Λ .
- 7.16 Size effects on phonon heat conduction across a spherical thin shell. Apply the ballistic-diffusive equations to solve the problem of steady-state phonon heat conduction between a spherical thin shell of thickness d . The inner and the outer surfaces are maintained at T_i and T_o , respectively. Phonon mean free path in the parent bulk material of the shell is Λ .
- 7.17 Size effects on heat conduction with an internal heat source: ballistic-diffusive treatment. Heat is uniformly generated inside a nanoscale spherical region of diameter d , embedded inside an infinite medium. The heat generation region and the surrounding are of the same material with no boundary; that is the transmissivity is equal to one. Use the ballistic-diffusive approximation to solve for the temperature profile inside the surrounding medium. Phonon mean free path in the surrounding medium is Λ .
- 7.18 Size effects on heat conduction with internal heat source: diffusion-transmission interface condition. Heat is uniformly generated inside a nanoscale spherical region of diameter d , embedded inside an infinite medium. Use the diffusion-transmission boundary condition to derive a simple expression for the

temperature dis
 assuming that t
 mean free path
 7.19 Size effects on
 diffusion appro
 condition to so
 thickness d . De
 shell. Bulk pho
 outer surfaces o
 7.20 Size effects on
 the diffusion ap
 condition to sol
 shell of thickne
 of the thin shell
 inner and the o
 in the figure
 diffuse and
 at both in
 given.

Add the figure



spheres. Apply the modified radiative heat transfer between different temperatures T_1 and T_2 . The shells is absorbing, emitting,

cylinders. Apply the modified radiative heat transfer between different temperatures T_1 and T_2 . In the cylinders is absorbing,

thin shell. Apply the ballistic-state phonon heat conduction. Derive an expression for the transient equilibrium temperatures respectively. Phonon mean free

spherical thin shell. Apply the state of steady-state phonon heat conduction. The inner and the outer Phonon mean free path in the

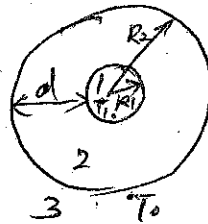
heat source: ballistic-diffusive nanoscale spherical region of material. The heat generation region with no boundary; that is the ballistic-diffusive approximation to solve the problem in the surrounding medium. Phonon mean free

source: diffusion-transmission approximation inside a nanoscale spherical region in an infinite medium. Use the diffusion approximation to derive a simple expression for the

temperature distribution inside the sphere as well as in the surrounding medium, assuming that the transmissivity at the interface is equal to one. Bulk phonon mean free path in both media is Λ .

7.19 *Size effects on phonon heat conduction across a spherical thin shell.* Use the diffusion approximation together with the diffusion-transmission boundary condition to solve for phonon heat conduction across a spherical thin shell of thickness d . Derive an expression for the effective thermal conductivity of the shell. Bulk phonon mean free path in the thin shell material is Λ . The inner and outer surfaces of the shell are maintained at T_i and T_o , respectively.

7.20 *Size effects on phonon heat conduction across a cylindrical thin shell.* Use the diffusion approximation together with the diffusion-transmission boundary condition to solve the problem of phonon heat conduction across a cylindrical thin shell of thickness d . Derive an expression for the effective thermal conductivity of the thin shell. Bulk phonon mean free path in the thin shell material is Λ . The inner and the outer surfaces are maintained at T_i and T_o , respectively, as shown in the figure. Phonon scattering at both interfaces are diffuse and frequency independent. Transmissivities from at both interfaces from each side to the other are given.



phonon transmissivity
 τ_{12}, τ_{21}
 τ_{23}, τ_{32}

Figure for P7.19 and P7.20.

Add the paragraph to both 7.19 & 7.20. Share one figure. Fig. is given in solution

same

$$n_{\mathbf{q}} + 1) \delta(E_{\mathbf{k}} - E_{\mathbf{k}-\mathbf{q}} - \hbar\omega) \tag{8.19}$$

ent inelastic and elastic scattering ct that the summation over \mathbf{q} is ld function of \mathbf{k} . Equation (8.19) m has the typical *relaxation time*

$$\delta(E_{\mathbf{k}} - E_{\mathbf{k}-\mathbf{q}} - \hbar\omega) \tag{8.20}$$

assume detailed expressions for distributions but that the phonons respectively,

$$= \frac{1}{\exp\left(\frac{\hbar\omega}{\kappa_B T_p}\right) - 1} \tag{8.21}$$

n into integration,

$$1 - f_{\mathbf{k},0} \left[-\hbar v_e q \cos \theta - \frac{\hbar^2 q^2}{2m} + \hbar\omega \right] \tag{8.22}$$

er high-temperature situations

2), we will use the following

$$x_0 > b \tag{8.24}$$

that the $\cos \theta$ in the first delta for θ within $[0, \pi/2)$, and to

negative values, that is, for θ within $(\pi/2, \pi]$, in the second delta function. Both these delta functions set the minimum of q , q_{\min} , to zero and the maximum of q , q_{\max} , to $2mv_e/\hbar$. Equation (8.22) can thus be written as

$$\frac{1}{\tau} = \left(\frac{1}{4\pi^2}\right) \int_0^{2mv_e/\hbar} q^2 dq \times \left(\frac{\pi Z_A^2 \omega}{\rho v_s^2}\right) \left(\frac{\kappa_B T_p}{\hbar\omega}\right) \times (2 - f_{\mathbf{k}+\mathbf{q},0} - f_{\mathbf{k}-\mathbf{q},0}) \frac{1}{\hbar v_e q} \tag{8.25}$$

For semiconductors that are not heavily doped, the Fermi level is typically inside the bandgap, so that $f_{\mathbf{k}+\mathbf{q},0}$ and $f_{\mathbf{k}-\mathbf{q},0}$ is much smaller than one and can be neglected. In this case, eq. (8.25) can be explicitly integrated, leading to

$$\begin{aligned} \frac{1}{\tau} &= \left(\frac{Z_A^2}{\pi \rho v_s^2}\right) \left(\frac{\kappa_B T_p}{\hbar^4}\right) m^2 v_e \\ &= \frac{\sqrt{2} \kappa_B m^{3/2} Z_A^2 T_p}{\pi \rho v_s^2 \hbar^4} E^{1/2} \end{aligned} \tag{8.26}$$

This expression is valid for electron scattering with longitudinal acoustic phonons in a semiconductor at high temperature, that is, when the lattice temperature is higher than the Debye temperature. For metals, the relaxation time due to longitudinal acoustic phonons is different from the above expression because (1) $f_{\mathbf{k}+\mathbf{q},0}$ and $f_{\mathbf{k}-\mathbf{q},0}$ are no longer negligible and (2) the upper limit for q is no longer $2mv_e/\hbar$ since the latter is much larger than the maximum allowable wavevector of the first Brillouin zone. A detailed treatment of relaxation time due to electron and acoustic phonon scattering in metals was given by Wilson (1953), and it is found that

$$\frac{1}{\tau} = \frac{3(6\pi^5)^{1/3}}{16\sqrt{2}} \frac{\kappa_B Z_A^2 T_p}{\sqrt{m} \rho v_s^2 a^4} E^{-3/2} \tag{8.27}$$

where a is the length of the unit cell.

We now turn our attention to inelastic scattering term, eq. (8.18). We follow a similar derivation as for the relaxation time τ and again limit the derivations to the longitudinal acoustic phonon scattering of electrons in semiconductors. Equation (8.18) can be expressed as

$$\begin{aligned} \left(\frac{\partial f}{\partial t}\right)_{c,i} &= \frac{1}{4\pi^2} \int_0^{2mv_e/\hbar} q^2 dq \left(\frac{\pi Z_A^2 \omega}{\rho v_s^2}\right) \frac{1}{\hbar q v_e} n_{\mathbf{q}} f_0(E) \exp\left(\frac{E - E_f}{\kappa_B T_e}\right) \\ &\times \left[\left[f_0(E + \hbar\omega) - f_0(E - \hbar\omega) \exp\left(-\frac{\hbar\omega}{\kappa_B T_e}\right) \right] \right. \\ &\left. \left[\exp\left(\frac{\hbar\omega}{\kappa_B T_p}\right) - \exp\left(\frac{\hbar\omega}{\kappa_B T_e}\right) \right] \right] \end{aligned} \tag{8.28}$$

Assuming that $\kappa_B T_e$ and $\kappa_B T_p$ are much larger than $\hbar\omega$, and also assuming $(E - E_f) \gg \kappa_B T_e$, we can approximate the above equation to

2/21/06. From (8.26) & (8.25), for non-degenerate semiconductors, we get

$$\mu_e = \frac{e Z m}{m} = \frac{8e}{3m} \times \frac{\pi \rho v_s^2 \hbar^4}{\sqrt{2} \kappa_B m^{3/2} Z_A^2 T_p} \frac{1}{\sqrt{\kappa_B T}}$$

$$\begin{aligned}
 \left(\frac{\partial f}{\partial t}\right)_{c,i} &\approx f_0 \frac{1}{4\pi^2} \int_0^{2mv_e/\hbar} n_{\mathbf{q}} q dq \left(\frac{\pi Z_A^2 \omega}{\hbar v_e \rho v_s^2}\right) \left(\frac{\hbar \omega}{\kappa_B T_p} - \frac{\hbar \omega}{\kappa_B T_e}\right) \left[1 - \exp\left(-\frac{\hbar \omega}{\kappa_B T_e}\right)\right] \\
 &= f_0 \frac{1}{4\pi^2} \int_0^{2mv_e/\hbar} q dq \frac{\kappa_B T_p}{\hbar \omega} \left(\frac{\pi Z_A^2 \omega}{\hbar v_e \rho v_s^2}\right) \left(\frac{\hbar \omega}{\kappa_B T_p} - \frac{\hbar \omega}{\kappa_B T_e}\right) \frac{\hbar \omega}{\kappa_B T_e} \\
 &= \frac{2\sqrt{2} m^{5/2} Z_A^2 E^{3/2}}{\pi \rho \hbar^4 \kappa_B T_e^2} f_0 (T_e - T_p) = g (T_e - T_p) \tag{8.29}
 \end{aligned}$$

where the factor g can also be related to the relaxation time in eq. (8.26),

$$g = \frac{2\sqrt{2} m^{5/2} Z_A^2 E^{3/2}}{\pi \rho \hbar^4 \kappa_B T_e^2} f_0 = \frac{2mv_s^2 E f_0}{\kappa_B^2 T_e^2 T_p \tau} \tag{8.30}$$

This expression shows that $(\partial f/\partial t)_{c,i}$ represents the inelastic scattering that drives the electrons and phonons to equilibrium. For metals, Qiu and Tien (1993) derived the following expression,

$$\left(\frac{\partial f}{\partial t}\right)_{c,i} = \frac{3\pi^2}{2\sqrt{2}} \left(\frac{3}{4\pi}\right)^{1/3} \frac{\sqrt{m} Z_A^2 E^{-1/2}}{\kappa_B \rho \dot{\alpha}^4} f_0 (1 - f_0) \left(f_0 - \frac{1}{2}\right) \frac{T_e - T_p}{T_e^2} \tag{8.31}$$

Equation (8.31) describes the energy loss trends in metals. If the electron energy is higher than the Fermi level ($f_0 < \frac{1}{2}$), the term is negative, indicating that electrons are losing high-energy carriers because of their collision with the lattice. If the electron energy is lower than the Fermi level ($f_0 > \frac{1}{2}$) the scattering tends to supply carriers to these states. In contrast, eq. (8.27) represents an elastic scattering process. One can understand this statement by multiplying both sides of the Boltzmann equation by energy and integrating over all allowable energy states. The two scattering terms are

$$\sum_{\mathbf{k}} E \left(\frac{\partial f}{\partial t}\right)_{c,e} = 0 \tag{8.32}$$

$$\sum_{\mathbf{k}} E \left(\frac{\partial f}{\partial t}\right)_{c,i} = G (T_e - T_p) \tag{8.33}$$

where G is called the electron-phonon coupling factor. From eq. (8.29), the electron-phonon coupling factor due to acoustic phonon scattering in nondegenerate semiconductors (such that the Boltzmann statistics is valid) is

$$\begin{aligned}
 G &= \sum_{\mathbf{k}} E \left(\frac{\partial f}{\partial t}\right)_{c,i} = \int_0^\infty E g D(E) dE = \frac{n \int_0^\infty E g D(E) dE}{\int_0^\infty f_0 D(E) dE} \\
 &= \frac{2\sqrt{2} n m^{5/2} Z_A^2}{\pi \rho \hbar^4 \kappa_B T_e^2} \frac{\int_0^\infty E^3 \exp\left(-\frac{E-E_f}{\kappa_B T_e}\right) dE}{\int_0^\infty E^{1/2} \exp\left(\frac{E-E_f}{\kappa_B T_e}\right) dE} \\
 &= \frac{12\sqrt{2} n m^{5/2} Z_A^2}{\pi^{3/2} \rho \hbar^4 T_e} (\kappa_B T_e)^{3/2} \tag{8.34}
 \end{aligned}$$

2/21/06 use μ_e in prev page

$G = \frac{32}{\pi^{3/2}} \frac{n m^{5/2} v_s^2}{\rho \hbar^4 T_e} = \frac{32}{\pi^{3/2}} \frac{n e v_s^2}{\rho \hbar^4 T_e}$ which is close to (8.36)

where n is the electron density in the parabolic band for electrons, we see that the energy loss per electron is thus

The above result differs from eq. (8.29) by a factor of $2/3$.

The electron-phonon coupling factor was first derived by researchers (Kaganov et al., 1957) gave the following expression for temperatures in metal

where the electron relaxation time τ_e is given by We should remind you that the same relation also holds true for holes

This can be proven from the Boltzmann equation using the approximations invoked in the derivation of the carrier conservation equation

The above derivation can also carry out similar for hole scattering term due to acoustic phonon scattering (1960; Srivastava, 1990)

$$\left(\frac{\partial n_{\mathbf{q}}}{\partial t}\right)_c = \frac{4\pi n_{\mathbf{q}}}{\hbar} \left(\frac{\partial f}{\partial t}\right)_c$$

One should be able to derive the above expression for the electron-phonon coupling term. The energy loss of electrons to phonons is given by

Equation (8.20) shows that the energy loss of electrons to phonons satisfies $\mathbf{k} - \mathbf{k}' = \mathbf{q}$. The energy loss of electrons to phonons is an average. Solving for the energy loss implies that scattering is not very good. For example

be approximated by the Boltzmann distribution, we derived in example 6.1 an expression for the Seebeck coefficient, from which the Peltier coefficient can be expressed as

$$\begin{aligned} \Pi_n &= \frac{T\kappa_B}{e} \left[\frac{\psi_e - E_c}{\kappa_B T} - \left(\gamma_e + \frac{5}{2} \right) \right] \\ &= + \frac{E_{fe}}{e} - \left(\gamma_e + \frac{5}{2} \right) \frac{\kappa_B T}{e} \end{aligned} \quad (8.114)$$

where γ_e is the parameter in the energy dependence of the electron scattering ($\sim E^{\gamma_e}$).

In region B-D, E_c is a constant. If we further consider an isothermal condition, consistent with Shockley's derivation, the first term in eq. (8.113) can be expressed as

$$\begin{aligned} \dot{q}_n(x_B \leq x \leq x_D) &= - \frac{[E_c + (\gamma_e + 5/2)\kappa_B T] dJ_e}{e dx} \\ &= \left[E_c + \left(\gamma_e + \frac{5}{2} \right) \kappa_B T \right] \frac{n - n_{p0}}{\tau_e} \\ &= \left[E_c + \left(\gamma_e + \frac{5}{2} \right) \kappa_B T \right] \frac{n_{p0}}{\tau_e} \left[\exp \left[\frac{eV}{\kappa_B T} \right] - 1 \right] \exp \left(- \frac{x - x_B}{L_e} \right) \end{aligned} \quad (8.115)$$

To evaluate the second term in eq. (8.113), we start from the fact that the total electron and hole current at each location must be a constant, and thus

$$\nabla J_e(x) = -\nabla J_p(x) \quad (8.116)$$

Thus the second term in eq. (8.113) is

$$\begin{aligned} \dot{q}_p(x_B \leq x \leq x_D) &= -(\Pi_h - \psi_h/e) \frac{dJ_e}{dx} \\ &= \left[-E_v + \left(\gamma_h + \frac{5}{2} \right) \kappa_B T \right] \frac{n_{p0}}{\tau_e} \left[\exp \left(\frac{eV}{\kappa_B T} \right) - 1 \right] \\ &\quad \exp \left(- \frac{x - x_B}{L_e} \right) \end{aligned} \quad (8.117)$$

where Π_h is the Peltier coefficient for holes and γ_h is the parameter in the energy dependence of the hole scattering. The total energy source term in the region $x_B < x < x_D$ is therefore

$$\begin{aligned} \dot{q}(x) &= \left[E_c - E_v + \left(\gamma_h + \frac{5}{2} \right) \kappa_B T \right. \\ &\quad \left. + \left(\gamma_e + \frac{5}{2} \right) \kappa_B T \right] \frac{n_{p0}}{\tau_e} \left[\exp \left(\frac{eV}{\kappa_B T} \right) - 1 \right] \exp \left(- \frac{x - x_B}{L_e} \right) \\ &= \left[E_c - E_v + \left(\gamma_h + \frac{5}{2} \right) \kappa_B T + \left(\gamma_e + \frac{5}{2} \right) \kappa_B T \right] \frac{n - n_{p0}}{\tau_e} \end{aligned} \quad (8.118)$$

This is the energy inside the square b : E_g , while the rest currents. This energy remembered that so particularly in direct based devices, most as heat.

We can integrate this section,

$$\begin{aligned} \dot{Q}_{BD} &= \left[E_g + \left(\dots \right) \right] \\ &= - \left[E_g + \left(\dots \right) \right] \end{aligned}$$

where the negative sign where the negative sign energy released in region

$$\dot{Q}_{CA} = - \left[\dots \right]$$

The total energy released C-A and B-D is then

$$\dot{Q}_{CA-BD} = \dots$$

This energy released supplied by the external the extra energy coming region. In this region J_p are constant. However we have

$$\dot{q}(x_A) = \dots$$

The profile of E_c and appendix B). The solution the energy source term Integrating eq. (8.122)

$$\dot{Q} = \dots$$

Another parameter that is useful for refrigeration performance is the maximum temperature difference that a given system can ideally reach. The maximum temperature difference is reached when there is no net cooling power taken from the source. Therefore, the coefficient of performance is zero at the maximum temperature difference. The corresponding maximum temperature difference can be obtained from eq. (8.132) as

$$(T_H - T_C)_{\max} = \frac{1}{2} ZT_C^2 \quad (8.142)$$

8.4.1.2 Thermoelectric Power Generation

The thermoelectric power generation mode can be analyzed similarly. In a power generation mode, as shown in figure 8.10(b), the heat supplied to the hot side should be

$$Q_H = (S_h - S_e)I_e T_H + K(T_H - T_C) - \frac{1}{2} I_e^2 R_e \quad (8.143)$$

and the power output is

$$W_e = I_e^2 R_L \quad (8.144)$$

where R_L is the external load resistance of the output circuit. The output current is given by

$$I_e = \frac{(S_h - S_e)(T_H - T_C)}{R_e + R_L} \quad (8.145)$$

Therefore, the thermal efficiency is

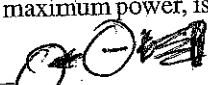
$$\eta = \frac{W_e}{Q_H} = \frac{I_e^2 R_L}{(S_h - S_e)I_e T_H + K(T_H - T_C) - \frac{1}{2} I_e^2 R_e} \quad (8.146)$$

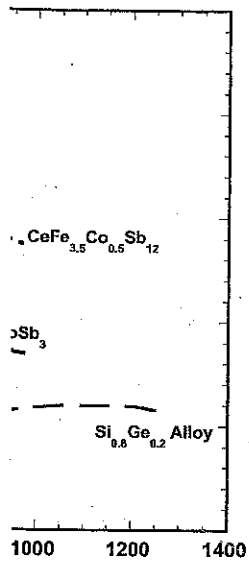
It can be shown that the maximum power is obtained with a matched load $R_L = R_e$. The maximum efficiency, which does not have to occur at the maximum power, is determined by setting $d\eta/dR_L = 0$,

$$\eta_{\max} = \frac{(T_H - T_C)(\sqrt{1 + ZT_M} + 1)}{T_H(\sqrt{1 + ZT_M} + T_C/T_H)} \quad (8.147)$$

Equations (8.141) and (8.147) show that one could make thermoelectric refrigerators and power generators close to the Carnot efficiency if materials with large ZT could be identified. The search for high ZT materials, however, has proven to be a very difficult path. The best ZT materials are found in heavily doped semiconductors. Insulators have poor electrical conductivities. Metals have relatively low Seebeck coefficients. In addition, the thermal conductivity of a metal, which is dominated by electrons, is proportional to the electrical conductivity, as dictated by the Wiedmann-Franz law [eq. (6.88)]. It is thus hard to realize high ZT in metals. In semiconductors, the thermal conductivity consists of contributions from electrons (k_e) and phonons (k_p), with the majority coming from phonons. The phonon thermal conductivity can be reduced without causing too

change "f" into "1"





s are for bulk materials and dots
 .3 has recently been reported on
 t al., 2003).

pproach to reduce the phonon
 mass difference scattering in
 tly without much degradation
 rials are alloys of Bi_2Te_3 with
 Bi_2Se_3 (such as $\text{Bi}_2\text{Te}_{2.7}\text{Se}_{0.3}$,
 qual to one (Goldsmid, 1964).
 1 and germanium, with a ZT

stly limited to bulk materials.
 ZT started to attract attention
 the research in bulk materials
 structures offer a chance of
 igh the use of quantum and
 been explored, such as quan-
 93; Dresselhaus et al., 2001)
 phonons (Chen et al., 2003;
 ce scattering and filtering of
 ons have both been explored
 1998; Zeng and Chen 2002).

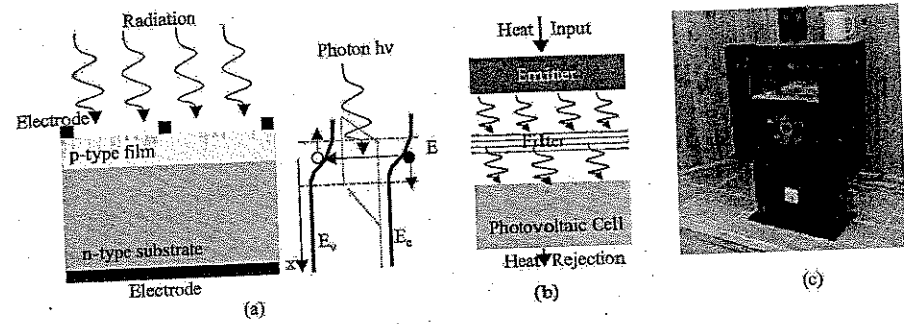


Figure 8.12 (a) The principle of a photovoltaic cell; (b) principle of thermophotovoltaic power generation; (c) a prototype thermophotovoltaic converter powered by a stove (Fraas et al., 2003; courtesy of Dr. L.M. Fraas).

Impressive ZT values have been reported in some superlattice structures based on both an enhancement of the electron performance (Harman et al., 2002) and a reduction in thermal conductivity (Harman et al., 2002; Venkatasubramanian, et al., 2001), with biggest benefit coming from the thermal conductivity reduction. Figure 8.11 shows a snapshot of the ZT of state-of-the art materials (Chen et al., 2003). The ZT of many nanostructures has surpassed that of bulk materials. However, these nanostructured materials are difficult to synthesize and useful devices have yet to be made from them. More information on nanostructured thermoelectric materials can be found in several reviews (Tritt, 2001; Chen and Shakouri, 2002; Chen et al., 2003).

8.4.2 Solar Cells and Thermophotovoltaic Power Conversion

8.4.2.1 Basic Principles

Solar cells (and, more generally, photovoltaic cells) absorb the photon energy from the sun and convert it into electricity (Chapin et al., 1954; Sze, 1981). The working principle of a solar cell comprising a p-n junction is sketched in figure 8.12(a). Photons from the sun generate electron-hole pairs in the space charge region. The electrostatic field in this region pulls holes to the p-type region and electrons to the n-type region. The accumulation of electrons and holes in these two regions generates a voltage. Thermophotovoltaic power generators are similar to photovoltaic cells but use a heat source to generate photons rather than solar energy (Coutts, 1999). A regular thermophotovoltaic device usually consists of the following parts: a heat source, an emitter to emit photons, a filter to reflect unwanted photons, photovoltaic cells to generate electricity, and a thermal management system to keep the photovoltaic cell cool, as shown in figure 8.12(b). Figure 8.12(c) is an example of a commercial thermophotovoltaic power generator powered by a furnace.

The p-n junction current as given by eq. (8.111) is balanced by the electron-hole generation rate

$$J_e = -J_s(e^{eV/k_B T} - 1) + J_g \tag{8.148}$$

where J_s is also called the dark current for diodes operated as photon detectors, and J_g is the current source due to photon absorption, which we will discuss later.

change "G" sub into "g"

Under an open-circuit condition, eq. (8.148) gives the open-circuit voltage of the photovoltaic cell as

$$\hookrightarrow V_0 = \frac{\kappa_B T}{e} \ln \left(\frac{J_g}{J_s} + 1 \right) \quad (8.149)$$

As eq. (8.112) shows, the dark current is dependent on the bandgap,

$$\hookrightarrow J_s = A \exp \left(-\frac{E_g}{\kappa_B T} \right) \quad (8.150)$$

where the coefficient A can be derived from eq. (8.112) for the Shockley ideal diode model. In Shockley's model, the dark current is due to nonradiative recombination outside the space charge region. A more fundamental limit is the radiative recombination (Shockley and Queisser, 1961; Henry, 1980) that must exist on the basis of the Kirchoff law in radiation; that is, the absorption must balance the emission for a system in equilibrium. This fundamental limit leads to the following expression for A (Henry, 1980),

Need more physical explanation

$$A \approx \frac{e(n^2 + 1)E_g^2 \kappa_B T}{4\pi^2 \hbar^3 c^2} \quad (8.151)$$

where n is the refractive index of the photovoltaic cell and c is the speed of light in vacuum. This A is typically much smaller than that due to nonradiative recombination as given by eq. (8.112). The dark current caused by radiative recombination is often used to estimate the maximum efficiency of a solar cell.

Substituting eq. (8.150) into (8.149), the open-circuit voltage ($J_e = 0$) can be expressed as

$$\hookrightarrow V_0 \approx \frac{E_g}{e} - \frac{\kappa_B T}{e} \ln \left(\frac{A}{J_g} \right) \quad (8.152)$$

which implies that the output voltage depends on the bandgap. The power output per unit area from a solar cell is

$$\hookrightarrow W_e = J_e V = -J_s V (e^{eV/\kappa_B T} - 1) + J_g V \quad (8.153)$$

and the maximum power output can be obtained from $dW_e/dV = 0$. This mathematical operation leads to the following expression for the optimum current and voltage,

$$\hookrightarrow J_{opt} = J_s \frac{eV_{opt}}{\kappa_B T} \exp \left[\frac{eV_{opt}}{\kappa_B T} \right] \approx J_g \left[1 - \frac{eV_{opt}}{\kappa_B T} \right] \quad (8.154)$$

$$V_{opt} = \frac{\kappa_B T}{e} \ln \left(\frac{J_g/J_s + 1}{1 + eV_{opt}/(\kappa_B T)} \right) \approx V_0 - \frac{\kappa_B T}{e} \ln \left(1 + \frac{eV_{opt}}{\kappa_B T} \right) \quad (8.155)$$

\hookrightarrow We now determine J_g , the current source due to photon excitation of electrons and holes. The radiation source is at temperature T_s . The quantity of photons entering the photovoltaic cell depends on the emissivity of the emitter ϵ_ω , the transmissivity of the medium between the emitter and the photovoltaic cell τ_ω , the reflectivity of the

ENE
40
30
20
10
0

Efficiency (%)

Figure 8.13 Maximum efficiency (as represented by C) solar Physics).

photovoltaic cell itself I photon entering the photo multiple reflection effect

\hookrightarrow J_g

where $I_{b\omega}/(\hbar\omega)$ is the ph of electrical power gene

The maximum efficiency figure 8.13 (Henry, 1980) is too large, there are fe the bandgap is too small

For a thermophotovo the net power leaving th

To maximize the effici bandgap and zero below systems is also address

High-Efficiency Solar Cell Based on 7-739.

of Solids, Academic Press, Orlando,

Large Radiative Transfer over Small Applications," *IEEE Transactions on*

Dover, New York, pp. 76-80.
 Ident Peltier Coefficient and Internal 56, pp. 1-11.

on Metals," *International Journal of*

as during Short-Pulse Laser Heating -841.

grated Thermionic Coolers," *Applied*

Bowers, J.E., 1998, "Thermoelectric scale Thermophysical Engineering,

Semiconductors and p-n Junction . 435-489.

hm's Law," *Bell System Technical*

Limit of Efficiency of p-n Junction 0-519.

r, Bristol, pp. 200-226.

igation of Heterojunction Transport i," *IEEE Transactions on Electron*

Semiconductor Barriers," *Physical*

b-Continuum Simulations of Heat nal of Heat Transfer, vol. 123,

lson, K. E., 2001b, "Measurement i," *Applied Physics Letters*, vol. 78,

Wiley, New York.

ials Research, *Semiconductors and*

ices with High Room-Temperature

t of Heat Generation and Conduc- tions on Computer-Aided Design,

id Device Physics, Prentice Hall,

ance of Microscale Thermophoto- i on Energy Conversion, vol. 17,

ress, Cambridge, UK.

ic Figure of Merit of Monopolar s, vol. 31, pp. 265-267.

Zeng, T., and Chen, G., 2000, "Energy Conversion in Heterostructures for Thermionic Cooling," *Microscale Thermophysical Engineering*, vol. 4, pp. 39-50.

Zeng, T., and Chen, G., 2002, "Interplay between Thermoelectric and Thermionic Effects in Heterostructures," *Journal of Applied Physics*, vol. 92, pp. 3152-3161.

Ziman, J.M., 1960, *Electrons and Phonons*, Clarendon Press, Oxford, chapter 5.

8.8 Exercises

8.1 *Electron mobility in semiconductors* (Bardeen and Shockley, 1950). On the basis of eqs. (8.26) and (6.85),

(a) derive an expression for the electron mobility of a nondegenerate semi-conductor due to acoustic phonon scattering;

(b) show that the mobility depends on temperature through $T^{-3/2}$;

(c) estimate the average momentum relaxation time in silicon due to acoustic phonon scattering. *at 300 K* *The sc deformation potential is 9.5 eV, density is 2.33 x 10³ kg/m³*

8.2 *Electron-phonon coupling factor of semiconductors*. Estimate the value of the electron-phonon coupling factor in silicon (due to acoustic phonon scattering) as a function of the electron temperature for a carrier concentration of 10^{17} cm^{-3} . Take a deformation potential value of 5 eV. *and sound velocity is 5000 m/s*

8.3 *Relationship between mobility and electron-phonon coupling factor*. Derive a relationship between the electron mobility and the electron-phonon coupling factor for semiconductors due to acoustic phonon scattering.

8.4 *Classical collision model* (Shockley, 1951; Wang, 1989). In an intuitive model of electron-phonon interaction, we treat the phonon as a particle having mass M . The phonon mass can be approximately modeled as the mass of a single atom. Consider collinear collision of an electron having mass m and momentum $p_{e,i}$ with a phonon of mass M initially at rest. Since the phonon mass is much larger than the electron mass, the electron will bounce back with a momentum $p_{e,f}$ while the phonon gains a momentum of $P_{p,f}$.

(a) On the basis of energy and momentum conservation, show that the amount of energy transport per collision from electron to phonon is

$$(\delta E)_{e \rightarrow p} = \frac{P_{p,f}^2}{2M} = \frac{(2p_{e,i})^2}{2m} = 2mv_e^2 = \frac{2(m)}{L} \kappa_B T_e$$

where v_e is the electron random velocity and we have used the relation $mv_e^2/2 = \kappa_B T_e/2$ (since we are dealing with one degree of freedom in a collinear system).

(b) Similarly, consider a phonon with an initial momentum $P_{p,i}$ colliding with an electron initially at rest, and show that the energy exchange per collision is

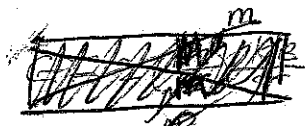
$$(\delta E)_{p \rightarrow e} = 2Mu^2 = \frac{2(M)}{L} \kappa_B T_p$$

(c) On the basis of the above results, show that the energy exchange rate between electron and phonon can be expressed as

$$\left(\frac{dE}{dt}\right)_c \approx G(T_e - T_p)$$

$$L \frac{2m}{M} \frac{\kappa_B}{\tau}$$

with $G = \frac{1}{\tau}$, where τ is the time interval between each collision, or the relaxation time.



- 8.5 *Electron-phonon coupling factor of metals.* Estimate the electron-phonon coupling factor in gold *when the lattice is at 300 K*
- 8.6 *Electron-hole pair generation due to light absorption.* Gallium antimonide (GaSb) is used as a photovoltaic cell material in thermophotovoltaic energy conversion. It is a direct gap semiconductor with a gap of 0.72 eV. The real part of the refractive index is 3.8. The absorption coefficient above the bandgap is $\sim 10^4 \text{ cm}^{-1}$. Determine the distribution of the electron-hole pairs for thermal radiation at normal incidence from a blackbody source of 1500 K.
- 8.7 *Hot electrons under a high field.* A voltage V is applied to an n-type semiconductor of length L between two electrodes, as shown in figure P8.7. The electron conductivity is σ and the electron-phonon coupling factor is G . We further assume that at the cathode, $x = 0$, the electrons and phonons are at the same room temperature. At the anode, the phonons are maintained at room temperature but the electrons' boundary condition is close to adiabatic (this is equivalent to assuming that the thermal conductivity and the Peltier coefficient of electrons in the anode are close to zero). The electron and phonon thermal conductivities of the semiconductor are k_e and k_p , respectively. Neglect thermoelectric effects.

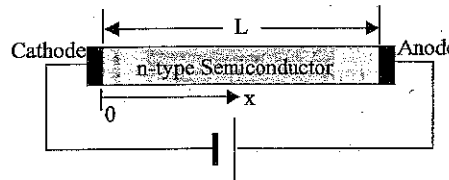
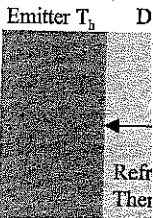


Figure P8.7 Figure for Problem 8.7.

Determine

- (a) the temperature distributions of electrons and phonons;
 - (b) the heat source distribution in the semiconductor.
- 8.8 *Heat generation in a p-n junction.* Consider a silicon p-n junction. The dopant concentrations for both the p and the n sides are 10^{18} cm^{-3} . The mobilities of electrons and holes are $170 \text{ cm}^2 \text{ V}^{-1} \text{ s}^{-1}$ and $60 \text{ cm}^2 \text{ V}^{-1} \text{ s}^{-1}$, respectively. The lifetimes of both electrons and holes are $\sim 10^{-10} \text{ s}$. The intrinsic carrier concentration n_i is $1.1 \times 10^{10} \text{ cm}^{-3}$. The bandgap of silicon is 1.12 eV.
- (a) Estimate the electron and the hole diffusion lengths.
 - (b) Estimate the saturation current density.
 - (c) Plot the heat source distribution due to electron-hole recombination in the n-type region.
- 8.9 *Heat source distribution under laser irradiation.* A laser beam with a wavelength of $1.55 \mu\text{m}$ and with an intensity of $10,000 \text{ W m}^{-2}$ is incident on a semiconductor with a bandgap of 0.66 eV and a complex refractive index of (4, 0.01). The electron-hole mobility is $1000 \text{ cm}^2 \text{ V}^{-1} \text{ s}^{-1}$ and the electron-hole recombination lifetime is 1 ms. Assuming that all recombination is nonradiative, determine the heat source distribution at steady state.
- 8.10 *Thermoelectric cooler.* Bismuth telluride (Bi_2Te_3) is a common thermoelectric material. State-of-the-art bulk n-type Bi_2Te_3 has the following properties: Seebeck coefficient, $-240 \mu\text{V K}^{-1}$; electrical resistivity, $10 \mu\Omega \text{ m}$; thermal conductivity, $2.2 \text{ W m}^{-1} \text{ K}^{-1}$

- (a) Calcul
 - (b) On the
 - the thermal co
 - (c) If, thro
 - be reduced to
 - electrical conc
 - (d) If a p-ty
 - maximum tem
 - made of the st
 - all properties a
- 8.11 *Thermophotov*
 photovoltaic c
 such that all pl
 are reflected b
 maximum effi
- 8.12 *Dielectric-cou*
 power output c
 between the e
 simplicity, we
 above the band
 that the photov
 bandgap back t

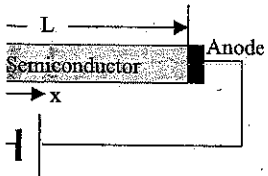


- (a) Show tha
- coupler than in v
- (b) Assuming
- the optimum ba
- maximum effici
- (c) If the die.
- no absorption, e
- function of the th
- Elaborate hov
- for (c). Assum
- there is no absor
- dielectric couple

LM

the electron-phonon
 300 K
 m. Gallium antimonide
 thermophotovoltaic energy
 gap of 0.72 eV. The real
 coefficient above the bandgap
 electron-hole pairs for thermal
 of 1500 K.

ed to an n-type semicon-
 ductor figure P8.7. The electron
 factor is G . We further
 phonons are at the same
 in at room temperature
 atic (this is equivalent to
 coefficient of electrons in
 thermal conductivities of
 thermoelectric effects.



ons;
 p-n junction. The dopant
 concentration is 10^{23} . The mobilities of elec-
 trons and holes are 10^3 and 10^1 ,
 respectively. The life-
 time of the carrier concentration
 is 10^{-8} s.

sole recombination in the
 semiconductor.
 beam with a wavelength
 identical on a semiconductor
 with a refractive index of (4, 0.01). The
 electron-hole recombination
 is radiative, determine the

is a common thermo-
 electric material with the following properties:
 Seebeck coefficient, $10 \mu\Omega$ m; thermal

- (a) Calculate the figure of merit of this material.
- (b) On the basis of the Wiedmann-Franz law and the Lorentz number, separate the thermal conductivity contributions due to electrons and to phonons.
- (c) If, through the use of nanostructures, the phonon thermal conductivity can be reduced to $0.25 \text{ W m}^{-1} \text{ K}^{-1}$ without degrading the Seebeck coefficient or the electrical conductivity, what figure of merit can one get?
- (d) If a p-type material with identical properties can also be obtained, calculate the maximum temperature difference that can be generated with a thermoelectric device made of the state-of-the-art material and the nanostructured material. Assume that all properties are temperature independent.

8.11 *Thermophotovoltaic generator.* Assuming that the photovoltaic cell of a thermophotovoltaic converter has a refractive index of 4 and that the filter is ideal, such that all photons above the bandgap are absorbed and all below the bandgap are reflected back to the heat source, determine the optimum bandgap and the maximum efficiency of the generator as a function of the emitter temperature.

8.12 *Dielectric-coupled thermophotovoltaic generator.* One idea to increase the power output of a thermophotovoltaic generator is to place a dielectric material between the emitter and the photovoltaic cell, as shown in figure P8.12. For simplicity, we assume that the refractive indices of all three media are matched above the bandgap of the photovoltaic cell and are equal to 4. We further assume that the photovoltaic cell has a built-in filter that reflects all radiation below the bandgap back to the emitter.

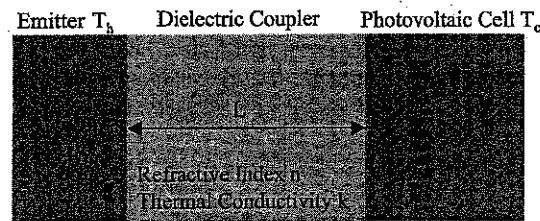


Figure P8.12 Figure for Problem 8.12.

- (a) Show that the blackbody radiation heat flux is n^2 higher in the dielectric coupler than in vacuum, where n is the refractive index.
 - (b) Assuming that the dielectric coupler has zero thermal conductivity, determine the optimum bandgap as a function of the emitter temperature and evaluate the maximum efficiency of the thermophotovoltaic system.
 - (c) If the dielectric coupler has a thermal conductivity $k = 1 \text{ W m}^{-1} \text{ K}^{-1}$ but no absorption, evaluate the maximum efficiency for a heat source at 1000°C as a function of the thickness of the coupler.
- Elaborate how absorption inside the dielectric coupler will affect the result for (c). Assume that the absorption coefficient above the bandgap is α and there is no absorption below the bandgap; also neglect the re-emission of the dielectric coupler.

where $x(t)$ and $r(t)$ are the instantaneous position of the particle. Thus, from measuring the mean displacement of the solute, the diffusivity can be determined.

In addition to the above approach, Einstein established another method to determine the diameter of solute particles. He proposed to measure the viscosity of the solvent and of the solution, μ_0 , and μ , respectively, and derived, again assuming dilute solute particles, the following relationship between the two viscosities,

$$\frac{\mu}{\mu_0} = 1 + 2.5\varphi = 1 + 2.5n\frac{1}{6}\pi D^3 \quad (9.35)$$

where φ is the volumetric concentration of the solute particles. We will not repeat Einstein's derivation but instead refer the reader to his original work (1906a; 1956). This result again applies only to dilute solutes. Many studies have been done to extend his results to higher volumetric concentrations (Hiemenz, 1986). These works should be a good starting point to examine recent claims on the novel properties of nanoparticle-seeded fluids, also referred to as nanofluids (Choi et al., 2001).

The Einstein relation can also be derived from the stochastic approach developed by Langevin to treat Brownian motion of particles much larger than those of the surrounding medium. The key idea of the Langevin equation is to assume that the motion of a Brownian particle is subject to a frictional force that is linearly proportional to its velocity, as in the Stokes law [eq. (9.28)], and a random driving force, $\mathbf{R}(t)$, imparted by the random motion of the molecules in the bath. The requirement that the Brownian particle is much larger in size than the molecules in the bath implies that the collision time of the bath molecules with the Brownian particle is much shorter than the relaxation time of the Brownian particle from its initial velocity, and hence there is no time correlation between the Brownian particle velocity and the molecular velocity. In the absence of an external force, the Langevin equation that governs the instantaneous velocity of the Brownian particle can be written as

$$m \frac{d\mathbf{u}}{dt} = -m\eta\mathbf{u} + \mathbf{R}(t) \quad (9.36)$$

where η is the friction coefficient for Brownian particles in a fluid. The Stokes law gives $\eta = 3\pi D\mu/m$. The random driving force $\mathbf{R}(t)$ has the following characteristics:

$$\langle \mathbf{R}(t) \rangle = 0 \quad (9.37)$$

$$\langle \mathbf{R}(t) \cdot \mathbf{u}(t) \rangle = 0 \quad (9.38)$$

$$\langle \mathbf{R}(t+s) \cdot \mathbf{R}(s) \rangle = 2\pi R_0\delta(t) \quad (9.39)$$

where the bracket $\langle \rangle$ represents the ensemble average, a concept we discussed in chapter 4. Equation (9.37) indicates that the random driving force averages to zero because it acts in all directions. Equation (9.38) states that the random driving force is not correlated to the velocity of the Brownian particle. This can be justified if the Brownian particle size is large and its velocity relaxation time is much longer than the characteristic fluctuation time of the random driving force. Equation (9.39) implies that the autocorrelation of the random driving force is infinitely short.

Now, we show
the inner product of
Brownian particle,

we obtain

By ensemble average,
out because there is
random driving force

we obtain from eq.

The initial condition

Equation (9.43) can

At large times such t

Combining eq. (9.47)

This is identical to eq.

From the Langevin
coefficient. We start
Strictly speaking, be
is problematic from a
spectral analysis of t

where $(-d\psi/dx)$ gives the electric field and $\rho_n(-d\psi/dx)$ gives the electrostatic force. Again, substituting in the Boltzmann distribution for charge, we can write the above equation as

$$dp = -d\psi \sum_i Z_i e n_{0i} \exp\left(-\frac{Z_i e \psi}{\kappa_B T}\right) \quad (9.66)$$

The above equation can be integrated, from infinity where $p = p_\infty$ and $\psi = 0$, leading to

$$\begin{aligned} p(x) - p_\infty &= \sum_i n_{0i} \kappa_B T \left[\exp\left(-\frac{Z_i e \psi(x)}{\kappa_B T}\right) - 1 \right] \\ &= \sum_i \kappa_B T [n_i(x) - n_{0i}] \end{aligned} \quad (9.67)$$

The right-hand side of eq. (9.67) is always positive and thus the pressure inside the electric double layer is higher than that inside the bulk liquid at the equilibrium state.

anion When the surface potential is negative, the *cation* concentration in the liquid near the surface is in excess of its equilibrium distribution far away from the surface and the *anion* concentration is smaller than its equilibrium distribution. The net effect is that the electric double layer creates an attraction force between the ions on the solid surface and the counterions in the liquid. This attractive electrostatic force is balanced by the positive pressure in the liquid.

Hence, when two solid surfaces are brought close to each other as shown in figure 9.7(b), a repulsive force develops between the two surfaces because the electrostatic force between the liquid and the solid surfaces no longer balances the positive pressure inside the liquid. A detailed exact solution for the symmetric surface case with only one type of counterions in the liquid has been obtained without invoking the Debye-Hückel approximation (Israelachvili, 1992). In this case, the potential distribution and the repulsive pressure between the two surfaces are given by

$$\exp\left(-\frac{Ze\psi}{\kappa_B T}\right) = \frac{1}{\cos^2 Kx} \quad (9.68)$$

$$p(D) = \kappa_B T n_0(D) = 2\epsilon_0 \epsilon_r \left(\frac{\kappa_B T}{Ze}\right)^2 K^2 \quad (9.69)$$

where n_0 is the counterion number density at the middle plane when the two surfaces are separated by a distance D , and $1/K$ is of the same order as the Debye length. K and n_0 are determined by the surface charge density c_s ,

$$-\frac{2\kappa_B T K}{Ze} \tan\left(\frac{KD}{2}\right) = \frac{c_s}{\epsilon_0 \epsilon_r} \quad (9.70)$$

$$K^2 = \frac{(Ze)^2 n_0}{2\epsilon_0 \epsilon_r \kappa_B T} \quad (9.71)$$



Figure 9.8 A repulsive dis... than can surface tension.

As an example, consider per 0.6 nm^2) separated b is, $Z = 1$, eq. (9.70) give Nm^{-2} or 17 atm. On th two surfaces, based on fi Hamaker constant of 10 electrical double layer.

The repulsive force in discussed here and also (negative), leads to the con sive force means that me or a negative pressure, wl disjoining pressure can r spreading and phase-chan

Figure 9.8 shows an ex The vapor-liquid interfac if the additional liquid-vapor ing repulsive pressure (di double layer between the taking $D = 2d$, where d i density c_s , eq. (9.70) lead

Integrating eq. (9.90) once

$$+ C_2 \quad (9.94)$$

and $d\psi/dy = 0$, thus $C_2 = 0$.
The thickness of the electric double layer,

$$= -D/2 + \delta) - \zeta] \quad (9.95)$$

(we have neglected the thickness of the electric double layer, $y = -D/2 + \delta$, where the velocity is zero. Thus, eq. (9.95) defines the channel as

$$(9.96)$$

shown in figure 16(b). Because of the plate separation, the flow in the electric double layer, the effect of the shear.

We do not consider the fluid structure. A recent molecular dynamics study of the wall than the Poisson-Boltzmann nanochannels, suggesting that the structures.

We can easily appreciate this from its dependence on curvature. Since the radius of curvature is large compared to the channel width, it is reasonable to anticipate that the properties will be independent of size. Examples are surface tension and contact angle. In-depth discussion of the work of Hill (1963, 1964). We limit our discussion to the phase material exists in the system so

that the thermodynamic properties is independent of curvature. We consider a spherical droplet and the surrounding fluid pressure. In the limit of a flat state to another, the Laplace

$$(9.97)$$

Next, we eliminate some variables so that we can solve the above equation. Because each phase is in thermal equilibrium, we can use the Gibbs-Duhem equation [eq. (8.83)] for each of the bulk phases

$$s' dT - v' dp' + d\mu' = 0 \quad (9.98)$$

$$s'' dT - v'' dp'' + d\mu'' = 0 \quad (9.99)$$

where s and v are the entropy and volume per mole, respectively, and μ is the chemical potential. A similar equation, called the Gibbs equation, exists for the interface,

$$d\gamma = -s_i dT - \Gamma d\mu_i \quad (9.100)$$

where Γ is the number density of molecules per unit area at the surface of tension, s_i is the entropy per unit area, and μ_i is the chemical potential at the interface. Equations (9.97)–(9.100) form the basis for analysing the effects of curvature on thermodynamic properties. Which of the variables we choose to eliminate depends on whether the liquid or the vapor is inside the sphere, and what are the system constraints, that is, constant pressure or constant temperature. We discuss a few cases below.

9.4.1 Curvature Effect on Vapor Pressure of Droplets

First we consider a droplet system at constant temperature so that p'' is the pressure inside the liquid droplet. At equilibrium, since $\mu' = \mu'' = \mu_i = \mu$, eqs. (9.98) and (9.99) lead to

$$v' dp' = v'' dp'' \quad (9.101)$$

Substituting eq. (9.101) into (9.97) and eliminating p'' yields

$$d \left(\frac{2\sigma}{r} \right) = \frac{v' - v''}{v''} dp' \quad (9.102)$$

If we further assume $v' \gg v''$, the ideal gas law for the vapor phase, and that v'' (liquid) is independent of pressure, the above equation can be integrated, leading to the Kelvin equation

$$\ln \left(\frac{p'}{p_0} \right) = \frac{2\sigma}{r} \frac{v''}{RT} \quad (9.103)$$

where R is the universal gas constant and p_0 is the normal vapor pressure when the interface is flat ($r \rightarrow \infty$). This equation shows that the equilibrium vapor pressure increases as the liquid droplet radius decreases. For a given vapor pressure, smaller droplets tend to evaporate. Thus, in a mist of droplets of pure substance, the large droplets will grow at the expense of the small droplets since they have a lower vapor pressure.

at 300K

- 9.7 *Debye length*. Estimate the Debye length in water containing 0.01 mole of NaCl. The dielectric constant of water is 78.54.
- 9.8 *Liquid helium and disjoining pressure*. It is known that if liquid helium is placed in a beaker, it rapidly climbs up the walls and down the other side, and eventually leaves the container. This is caused by a negative Hamaker constant between the helium vapor and the container wall.
- (a) Show that the liquid helium film varies as a function of its thickness,

$$D = \left(-\frac{A}{6\pi\rho gH} \right)^{1/3}$$

- (b) The Hamaker constant between helium vapor and the container, made of CaF_2 , is -0.59×10^{-20} J. Estimate the liquid helium film height at a thickness of $D = 2$ nm. The density of liquid helium is 125 kg m^{-3} .
- 9.9 *Capillary rise of liquid in a tube*. In a small tube inserted into a liquid bath, the liquid rises above the height of the bath surface due to the surface tension if the contact angle is less than 90° (figure P9.9). Show that the height of the liquid column is

$$H = \frac{2\sigma \cos \theta}{(\rho_l - \rho_v) g r_i}$$

where ρ_l and ρ_v are the density of the liquid and its vapor and r_i is the inner radius of the capillary tube. For glass tubes with $r_i = 10 \mu\text{m}$, $100 \mu\text{m}$, and 1 mm , estimate the heights of water inside the tube ($\gamma = 72.8 \text{ mN m}^{-1}$). For water-glass interface, $\theta = 14^\circ$.

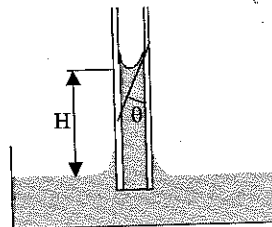


Figure P9.9 Figure for exercise 9.9.

- 9.10 *Electrokinetic flow*. Consider fully developed electro-osmotic flow between two parallel plates, assuming that the Debye thickness is much smaller than the separation of the two plates. Use the Hückel-Debye approximation to find the electric double layer potential distribution.
- (a) Develop an expression for the velocity distribution within the electric double layer.
- (b) Assuming that a constant heat flux is applied to the fluid on both surfaces and the thermal profile is fully developed, derive an expression for the Nusselt number.
- 9.11 *Effects of radius on water droplet surface tension and saturation vapor pressure*. For water, taking 9.6 \AA^2 as the surface area occupied by a water molecule on the surface of tension, half of the monolayer concentration is $\Gamma = 0.9 \times 10^{-9} \text{ mol cm}^{-2}$. The liquid phase density is $\rho'' = 5.55 \times 10^{-2} \text{ mol cm}^{-3}$. Calculate the surface tension and the saturation vapor pressure of water droplets as a function of the diameter in the range of $r = 10^{-9} - 10^{-6} \text{ m}$.

- 9.12 *Effects of pressure*. and the s its diam
- 9.13 *Melting* and solid the melti melting p
- 9.14 *Bismuth* sation of channels. process c bismuth i

at two different times, $t + \Delta t$

$$+ \Delta t) B(t) dt \quad (10.37)$$

ay Δt , but over time origin t . The all possible different time origins. $\langle B(t) \rangle$ is called the autocorrelation equal to the ensemble average,

$$\int_0^N \langle B(t) \rangle dt \quad (10.38)$$

the system.

Green's Relations

based on the kinetic theory of dilute functions of reduced order, such as an equation, which is an average equation, discussed in section 6.1, we have already pointed out some when applied to a dense medium response theory, developed in the (1) and others, which starts from (2) of the system to small external (3) general results for the system (4) viscosity, thermal conductivity, (5) the linearized Liouville equation. (6) lar dynamics simulation results. (7) as underlying it. Although this (8) molecular dynamics, the theory (9) erent.

(10) a Hamiltonian H_0 . The system (11) rnal force $F(t)$, which causes a (12) mption of a spatially homoge- (13) nclude spatial inhomogeneity (14) rbatation Hamiltonian $H'(t)$ can

$$(10.39)$$

(15) is, a function of the positions (16) olume of the system. We will (17) re interested in the response of

another phase variable, $B(\mathbf{r}, \mathbf{p})$, to this external force disturbance. In the linear response theory, this response will be linear to the force through an "after-effect function" $\phi_{BA}(t)$,

$$\langle B(t) \rangle = \int_{-\infty}^t \phi_{BA}(t-t') F(t') dt' = \int_0^{\infty} \phi_{BA}(\tau) F(t-\tau) d\tau \quad (10.40)$$

where we also assume that for the unperturbed case $\langle B_0 \rangle = 0$. The case when $\langle B_0 \rangle \neq 0$ (such as for internal energy and pressure) is only a simple extension. Equation (10.40) simply says that the response at time t is related to the previously applied force, as is required for all natural processes. This requirement is sometimes called causality. Since $F(t)$ and the response $\langle B \rangle$ are both real functions, the after-effect function $\phi_{BA}(t)$ must also be real. Our task is to derive expressions for $\phi_{BA}(t)$ that relate the response to the disturbance. This task will be accomplished in the next section. Here we will examine the properties of $\phi_{BA}(t)$ itself.

First, we introduce the temporal Fourier transformation of a function $F(t)$ and its inverse transformation,

$$F(t) = \int_{-\infty}^{\infty} \tilde{F}(\omega) e^{i\omega t} d\omega, \quad \tilde{F}(\omega) = \frac{1}{2\pi} \int_{-\infty}^{\infty} F(t) e^{-i\omega t} dt \quad (10.41)$$

Expressing the integrand of eq. (10.40) as the inverse of its Fourier transform, we can write

$$\begin{aligned} \langle B(t) \rangle &= \int_0^{\infty} \phi_{BA}(\tau) d\tau \left(\int_{-\infty}^{\infty} \left[\frac{1}{2\pi} \int_{-\infty}^{\infty} F(t''-\tau) e^{-i\omega t''} dt'' \right] e^{i\omega t} d\omega \right) \\ &= \int_0^{\infty} \phi_{BA}(\tau) \left[\int_{-\infty}^{\infty} \tilde{F}(\omega) e^{i\omega t} e^{-i\omega \tau} d\omega \right] \\ &= \int_{-\infty}^{\infty} d\omega \tilde{F}(\omega) e^{i\omega t} \int_0^{\infty} \phi_{BA}(\tau) e^{-i\omega \tau} d\tau \\ &= \int_{-\infty}^{\infty} \chi_{BA}(\omega) \tilde{F}(\omega) e^{i\omega t} d\omega \end{aligned} \quad (10.42)$$

The function $\chi_{BA}(\omega)$ is called the dynamic susceptibility or the response function,

$$\chi_{BA}(\omega) = \int_0^{\infty} \phi_{BA}(\tau) e^{-i\omega \tau} d\tau \quad (10.43)$$

and is generally a complex valued function,

$$\chi_{BA}(\omega) = \chi'_{BA}(\omega) + i\chi''_{BA}(\omega) \quad (10.44)$$

$$\begin{aligned}
 &= \int d\mathbf{r}_i d\mathbf{p}_i f^{(N)}(t, \mathbf{r}_i, \mathbf{p}_i) \left[\sum_{i=1}^N m \frac{\partial \delta(\mathbf{R} - \mathbf{r}_i(t))}{\partial \mathbf{r}_i} \frac{\partial \mathbf{r}_i}{\partial t} \right] \\
 &= - \int d\mathbf{r}_i d\mathbf{p}_i f^{(N)}(t, \mathbf{r}_i, \mathbf{p}_i) \left[\sum_{i=1}^N m \mathbf{v}_i \frac{\partial \delta(\mathbf{R} - \mathbf{r}_i(t))}{\partial \mathbf{r}_i} \right] \\
 &= - \frac{\partial}{\partial \mathbf{R}} \int d\mathbf{r}_i d\mathbf{p}_i f^{(N)}(t, \mathbf{r}_i, \mathbf{p}_i) \left[\sum_{i=1}^N m \mathbf{v}_i \delta(\mathbf{R} - \mathbf{r}_i(t)) \right] \\
 &= - \frac{\partial(\rho(t, \mathbf{R}) \bar{\mathbf{v}}(t, \mathbf{R}))}{\partial \mathbf{R}} \tag{10.97}
 \end{aligned}$$

where

$$\rho(t, \mathbf{R}) \bar{\mathbf{v}}(t, \mathbf{R}) = \sum_{i=1}^N m \mathbf{v}_i \delta(\mathbf{R} - \mathbf{r}_i(t)) \tag{10.98}$$

defines the velocity field $\bar{\mathbf{v}}$. Equation (10.97) is simply the equation of continuity,

$$\frac{\partial \rho}{\partial t} + \nabla \cdot (\rho \bar{\mathbf{v}}) = 0 \tag{10.99}$$

and $\rho \bar{\mathbf{v}}$ is the macroscopic mass flux. From eq. (10.98), we see that the macroscopic expression for the mass flux is

$$\mathbf{J}_m(t) = \sum_{i=1}^N m \bar{\mathbf{v}}_i \tag{10.100}$$

which is an apparent result. We can follow similar procedures for the time derivative of the momentum flux, $\rho \bar{\mathbf{v}}$, and compare the obtained expression with the macroscopic momentum conservation equation. This procedure leads to a microscopic expression for the shear stress tensor,

$$\tau_{xy} = \frac{1}{V} \left[\sum_i m (v_{xi} - \bar{v}_x)(v_{yi} - \bar{v}_y) + \frac{1}{2} \sum_{i=1}^N \sum_{j \neq i=1}^N x_{ij} \frac{\partial u(x_{ij})}{\partial y_{ij}} \right] \tag{10.101}$$

where x_{ij} and y_{ij} are the projections of \mathbf{r}_{ij} along the x - and y -directions, respectively. The above expression is valid only when the interatomic potential can be expressed as a pairwise sum, as in eq. (10.90). For a system in equilibrium, the average velocity is zero, that is, $\bar{\mathbf{v}} = 0$ (which will be assumed in all following expressions). Similar procedures also lead to a microscopic expression for the heat flux

$$\mathbf{J}_Q(t) = \frac{1}{V} \left[\sum_{i=1}^N \left(\mathbf{v}_i h_i + \frac{1}{2} \sum_{j=1, j \neq i}^N \mathbf{r}_{ij} (\mathbf{F}_{ij} \cdot \mathbf{v}_i) \right) \right] \tag{10.102}$$

where \mathbf{F}_{ij} is the force interaction between the pair of particles i and j . Again, the above expression is valid for pairwise potential only and modification should be made

for a three-body potential. Other methods of derivation have been developed (Hansen and McDonald, 1990). Among these methods, the approach leads to the heat flux (Hansen and

and

Although these simple methods are directly for simulation of molecular dynamics systems (Haile (1992).

10.3.6 Therm

In the linear response theory, canonical ensembles. In a time motion solved corresponds and number of particles, pressure and constant energy that in a constant pressure introduced a scaled system, from which scaled system, from which include the volume Π (to the rescaled coordinates average of a phase variable phase space coordinate ensemble with constant of the original system. V interest here is in the ca

Anderson himself w ensemble (constant N , the particles in the sim temperature. If we deno Δt of the numerical int going through the collision number to each particle particle goes through the

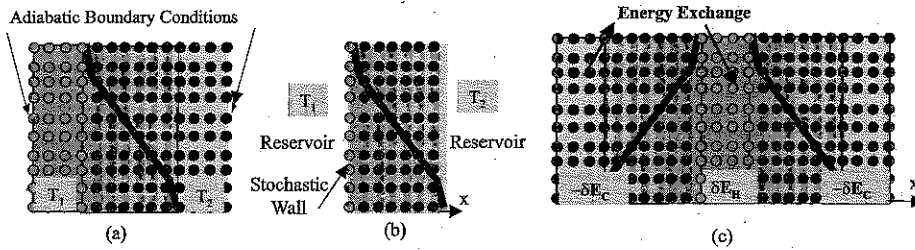


Figure 10.3 Different nonequilibrium molecular dynamics methods for simulating heat conduction: (a) constant temperatures are imposed in two regions of the simulation domain; (b) stochastic wall method; (c) heat flux method.

the thermal conductivity must be extrapolated to zero wavevector. Ciccotti et al. (1978) encountered some difficulty in such an extrapolation, which was addressed by Gillan and Dixon (1983). The latter authors showed that the revised scheme is equivalent to the results of the Green-Kubo method for a Lennard-Jones crystal. Evans (1982) developed a similar approach, however, without relying on direct computation of the perturbed heat flux. He argued that the Green-Kubo formula is not compatible with the periodic boundary condition because the equations of motion are discontinuous under this condition (Evans and Morriss, 1990). Evans called his method the homogeneous nonequilibrium molecular dynamics. There has not been any effort, however, to quantify the difference between the direct Green-Kubo formula-based simulation results and the homogeneous nonequilibrium molecular dynamics simulations, although Evans's paper (1982) shows that his method leads to excellent agreement with experimental data for argon crystals.

10.5.2 Nonequilibrium Molecular Dynamics Simulations

Nonequilibrium molecular dynamics methods are widely used to investigate fluid flow (Koplik and Banavar, 1995) and heat transfer processes (Chou et al., 1999; Maruyama, 2002). Due to the limitation on computational power, most nonequilibrium molecular dynamics simulations have so far been performed for one-dimensional heat conduction. In the lateral direction, periodic boundary conditions are often used. For heat transfer, two different approaches are taken to create the nonequilibrium transport conditions: impose a temperature difference to calculate the heat flux ($\Delta T \rightarrow Q$), or impose a heat flux to calculate the resulting temperature distributions ($Q \rightarrow \Delta T$). Within each of these categories, the actual implementation methods vary. We will discuss some of these methods.

Early works focused on the $\Delta T \rightarrow Q$ approach (Hoover and Ashurst, 1975; Levesque et al., 1973; Ciccotti and Tenenbaum, 1980; Tenenbaum et al., 1982). The key issue is how to impose the hot and cold reservoirs. Figures 10.3(a-c) illustrate various methods that have been used to impose hot and cold walls. In the hot and cold reservoir method [figure 10.3(a)], part of the simulation domain is designated as hot and the other part as cold. The average temperatures in the reservoirs are monitored and maintained as predetermined temperatures. Ashurst (1974) and Hoover and Ashurst (1975) designed

methods to maintain the method [Figure 10.3(b) Tenenbaum et al., 1982] the temperature difference by the following method simulation step and enter by sampling the following

$$f(v_y) = \left(\frac{m}{2\pi} \right)^{1/2} \exp\left(-\frac{mv_y^2}{2k_B T}\right)$$

$$f(v_x) = \frac{m}{k_B T} v_x \exp\left(-\frac{mv_x^2}{2k_B T}\right)$$

and its position is reassigned to a virtual reservoir. If this perturbation of the atom follows this newly assigned position, the stochastic wall by translation.

One concern with specifying a temperature difference is to come the problem, a corner (1994; Ikeshoji and Hafskjold) hot (or cold) regions by re-

where v'_i and v_i are the velocity, α is a scaling factor and β maintains zero so that the reservoirs are in each region. Energy conservation is maintained by setting ΔU negative

Equations (10.134–10.136) two symmetric regions are applied as a boundary condition to be applied to calculate the heat flux along the x -direction.

problems

Volz, S.G., Saulnier, J.B., Chen, G., and Beauchamp, P., 2000, "Computation of Thermal Conductivity of Si/Ge Superlattices by Molecular Dynamics Techniques," *Microelectronics Journal*, vol. 31, pp. 815-819.

Wang, X., and Xu, X., 2002, "Molecular Dynamics Simulation of Heat Transfer and Phase Change during Laser Material Interaction," *Journal of Heat Transfer*, vol. 124, pp. 264-274.

Wang, X., and Xu, X., 2003, "Molecular Dynamics Simulation of Thermal and Thermomechanical Phenomena in Picosecond Laser Material Interaction," *International Journal of Heat and Mass Transfer*, vol. 46, pp. 45-53.

Yang, C., Chen, M., and Guo, Z.Y., 2001, "Molecular Dynamics Simulation of the Specific Heat of Undercooled Fe-Ni Melts," *International Journal of Thermophysics*, vol. 22, pp. 1303-1309.

Zwanzig, R., 1965, "Time-Correlation Functions and Transport Coefficients in Statistical Mechanics," *Annual Review of Physical Chemistry*, vol. 16, pp. 67-102.

10.9 Exercises

10.1 Equations of motion for a constant pressure system. To simulate a constant pressure system, Anderson (1980) designed a scaled system with a Lagrangian of the form

$$L(\mathbf{r}', \dot{\mathbf{r}}', \Pi, \dot{\Pi}) = \frac{1}{2} m \Pi^{2/3} \sum_i \dot{\mathbf{r}}'_i \cdot \dot{\mathbf{r}}'_i - \frac{1}{2} \sum_{i=1}^N \sum_{j=1}^N u(\Pi r'_{ij}) + \frac{1}{2} M \dot{\Pi}^2 - \alpha \Pi$$

u is the internal energy

where α is the system pressure, and $\mathbf{r}'(t)$, $\dot{\mathbf{r}}'(t)$ and $\Pi(t)$ are related to the original system particle position $\mathbf{r}(t)$, momentum $\mathbf{p}(t)$, and volume $V(t)$ (volume fluctuates in a constant pressure ensemble) as follows,

$$\Pi(t) = V(t), \mathbf{r}'_i(t) = V(t)^{-1/3} \mathbf{r}_i(t), m \dot{\mathbf{r}}'_i(t) = V(t)^{-1/3} \mathbf{p}_i(t)$$

Answer the following questions:

- (a) What is the generalized momentum conjugate to Π ?
- (b) What is the Hamiltonian of the scaled system?
- (c) Derive the Hamiltonian equations of motion for the scaled system.
- (d) Derive the Lagrange equations of motion for the scaled system.

10.2 Linear response theory for particle mobility. If particles in a system are acted upon by an external force $\mathbf{F}(t)$, the Hamiltonian of the system is then

$$H = H_0 + \sum_i \mathbf{r}_i \cdot \mathbf{F}$$

where H_0 is the Hamiltonian of the unperturbed system. The particle mobility μ is defined in relation to the average velocity by

$$\langle \mathbf{v} \rangle = \mu \mathbf{F}$$

Derive the followi

where \mathbf{v} is the aver
10.3 Kramer-Kronig r
thermal conductivi

show that the real
relations.

10.4 Microscopic expres
sion for temperatu
microcanonical sys

where E is the sy
 $E = K + U$. The
Boltzmann principl

where Ω is the num
(Haile, 1992)

$$\Omega = \frac{1}{(2\pi\hbar)^3} \int \delta(E - H(\mathbf{p}, \mathbf{r})) d\mathbf{p} d\mathbf{r} = \left(\frac{m}{\hbar}\right)^3$$

where \hbar is the Planck
is a step function an
function. From here
the system kinetic en

10.5 Effects of Boundary
lation. To appreciate
dynamics simulation
film as shown in figur
for the following two
and varying the phor

10, "Computation of Thermal Techniques," *Microelectronics*

Heat Transfer and Phase Change, vol. 124, pp. 264-274.

Thermal and Thermomechanical *International Journal of Heat and*

Simulation of the Specific *Journal of Thermophysics*, vol. 22,

Transport Coefficients in Statistical *Journal of Applied Physics*, pp. 67-102.

m. To simulate a constant temperature system with a Lagrangian

$$\frac{1}{2} M \dot{\Pi}^2 - \alpha \Pi$$

$$-\frac{1}{2} M \dot{\Pi}^2 - \alpha \Pi$$

where Π is internal energy

and $\Pi(t)$ are related to the position, and volume $V(t)$ (volume

$$\rho = V(t)^{-1/3} \mathbf{p}(t)$$

Π ?

the scaled system.

the scaled system.

particles in a system are acted

on the system is then

tem. The particle mobility

Derive the following Green-Kubo formula for the particle mobility,

$$\mu = \frac{V}{3\kappa_B T} \int_0^\infty \langle \mathbf{v}(t) \cdot \mathbf{v}(0) \rangle dt$$

where \mathbf{v} is the average instantaneous velocity of all the particles in the system.

10.3 *Kramer-Kronig relation for thermal conductivity.* Given a frequency dependent thermal conductivity of the form

$$k(\omega) = \frac{k(0)}{-i\omega + 1/\tau}$$

show that the real and the imaginary parts of $k(\omega)$ obeys the Kramer-Kronig relations.

10.4 *Microscopic expression for temperature.* We can derive the microscopic expression for temperature from the thermodynamic definition of temperature in a microcanonical system,

$$\frac{1}{T} = \left(\frac{\partial S}{\partial E} \right)_{NV}$$

where E is the system energy, comprising a kinetic and a potential part, $E = K + U$. The entropy of a microcanonical system is, according to the Boltzmann principle,

$$S = \kappa_B \ln \Omega$$

where Ω is the number of microcanonical states, which can be expressed as (Haile, 1992)

$$\begin{aligned} \Omega &= \frac{1}{(2\pi\hbar)^{3N} N!} \int d\mathbf{r} d\mathbf{p} \theta(E - H) \\ &= \left(\frac{m}{\hbar} \right)^{3N/2} \frac{1}{N! \Gamma(3N/2 + 1)} \int d\mathbf{r} (E - U)^{\Gamma(3N/2)} \theta(E - H) \end{aligned}$$

where \hbar is the Planck constant divided by 2π , H is the system Hamiltonian, θ is a step function and its derivative is a delta function, and $\Gamma(N)$ is the gamma function. From here, show that temperature can be expressed as an average of the system kinetic energy

$$\frac{3}{2} \kappa_B T = N \langle K \rangle$$

10.5 *Effects of Boundary Conditions on Nonequilibrium Molecular Dynamics Simulation.* To appreciate the potential effects of hot and cold walls on the molecular dynamics simulation result, we consider phonon heat conduction across a thin film as shown in figure P10.5. Solve the phonon Boltzmann equation numerically for the following two boundary conditions, using the gray body approximation and varying the phonon Knudsen number from 0.01 to 100.

Conduction Band, E_c

Donor E_D (e.g. Phosphor)

Deep level

Acceptor E_A (e.g. Boron)

Valence Band, E_v

Appendix B

Semiconductor p-n Junctions

(b)

r. An electron is released from s boron in silicon) have energy nce band, becoming negatively rities (such as gold in silicon) ily do not contribute electrons mbination centers.

thus the electron and hole

(A11)

y electrons and N_D^+ is the Equation (A11) states that he crystal; this is called the lectrons in the conduction tron (thus creating a hole in rors and donors are given by

(A12)

(A13)

he donor, respectively, and state of the impurity level,

As shown in figure 8.7, when an n-type semiconductor and a p-type semiconductor are brought into physical contact, electrons in the n-type region diffuse into the p-type region, leaving positively charged ions (donors) behind. Similarly, holes diffuse into the n-type region, leaving negatively charged ions (acceptors) behind. At the interface, the positively charged ions in the n-side and the negatively charged ions in the p-side establish an electrostatic potential barrier that resists further diffusion to establish an equilibrium state for the whole structure. This is reflected in the band diagram shown in figure 8.7(b). The region around the interface where negatively and positively charged ions are no longer neutral is called the space-charge region. The concentration of free electrons or holes in this space-charge region is very low compared to the number of electrons and holes in the bulk material. The built-in potential over the space-charge region can be found from the requirements that the Fermi levels are equal at equilibrium and that, far away from the space-charge region, the free carrier concentrations must be the same as in homogeneous semiconductors. If we assume that both the donors in the n-type region and the acceptors in the p-type region are fully ionized, the electron concentration in the bulk n-type region, n_{n0} , that is, away from the space-charge region, is given by eq. (A3),

$$n_{n0} = N_D = N_c \exp\left(-\frac{E_{c1} - E_f}{\kappa_B T}\right) \quad (B1)$$

where E_{c1} is the level of the conduction band in the bulk n-type. The electron concentration in the bulk p-type region, n_{p0} , according to eqs. (A4) and (A7), is

$$n_{p0} = \frac{n_i^2}{p_{p0}} = N_c \exp\left(-\frac{E_{c2} - E_f}{\kappa_B T}\right) \quad (B2)$$

ns

Physical Constants

Physical constant	Symbol	Value	Units
Speed of light	c	2.997×10^8	m s^{-1}
Planck constant,	h	6.6262×10^{-34}	J s
Planck constant divided by 2π	\hbar	1.0546×10^{-34}	J s
Avogadro's number	N_A	6.0222×10^{23}	mol^{-1}
Electron rest mass	m	9.1096×10^{-31}	kg
Proton mass	m M	1.67×10^{-27}	kg
Proton mass/electron mass ratio		1836.1	
One electron volt	1 eV	1.6022×10^{-19}	J
Boltzmann constant	k_B	1.38×10^{-23}	J K^{-1}
Permittivity of free space	ϵ_0	8.8×10^{-12}	F m^{-1}
Permeability of free space	μ_0	$4\pi \times 10^{-7}$	$\text{s}^2 \text{F}^{-1} \text{m}^{-1}$
Stefan-Boltzmann constant	σ	5.67×10^{-8}	$\text{W m}^{-2} \text{K}^{-4}$
Ideal gas constant	R	8.314	$\text{J K}^{-1} \text{mol}^{-1}$
Lorentz number	L	$\sim 2.45 \times 10^{-8}$	$\text{W } \Omega \text{ K}^{-2}$
Universal ideal gas constant	R_u	8.314	$\text{J K}^{-1} \text{mol}^{-1}$

$$3 \text{ aJ} = 10^{21} \text{ yJ}$$

$$0^{-19} \text{ J} = 1.24 \text{ } \mu\text{m} \text{ (photon)}$$

$$= 26 \text{ meV}$$